

REPORT DOCUMENTATION PAGE

AFRL-SR-AR-TR-05-

0345

Public reporting burden for this collection of information is estimated to average 1 hour per response, including the time for gathering and maintaining the data needed, and completing and reviewing the collection of information. Send comments to Washington Headquarters Service, Directorate for Information Operations and Reports, 1215 Jefferson Davis Highway, Suite 1204, Arlington, VA 22202-4302, and to the Office of Management and Budget, Paperwork Reduction Project (0704-0188) Washington, DC 20503.

PLEASE DO NOT RETURN YOUR FORM TO THE ABOVE ADDRESS.

1. REPORT DATE (DD-MM-YYYY) 15-7-2005		2. REPORT TYPE Final		3. DATES COVERED (From - To) Feb 1 2002 to Jan 31 2005	
4. TITLE AND SUBTITLE Influence of Prepreg Microstructures on Structural Performance of Polymer Matrix Composites				5a. CONTRACT NUMBER	
				5b. GRANT NUMBER F49620-02-1-0098	
				5c. PROGRAM ELEMENT NUMBER	
6. AUTHOR(S) Dillon, Gregory P.				5d. PROJECT NUMBER	
				5e. TASK NUMBER	
				5f. WORK UNIT NUMBER	
7. PERFORMING ORGANIZATION NAME(S) AND ADDRESS(ES) Pennsylvania State University 110 Technology Center University Park, PA 16802				8. PERFORMING ORGANIZATION REPORT NUMBER AFOSR-GPD-7-15-2005	
9. SPONSORING/MONITORING AGENCY NAME(S) AND ADDRESS(ES) AFOSR/NL 875 Randolph Street Suite 325, Room 3112 Arlington, VA 22203-1954				10. SPONSOR/MONITOR'S ACRONYM(S) AFOSR	
				11. SPONSORING/MONITORING AGENCY REPORT NUMBER	
12. DISTRIBUTION AVAILABILITY STATEMENT Unrestricted				DISTRIBUTION STATEMENT A Approved for Public Release Distribution Unlimited	
13. SUPPLEMENTARY NOTES					
14. ABSTRACT This study provides methods by which composite prepreg materials can be characterized at the microscopic level. By applying established spatial tessellation schemes developed by Dirichlet, a means by which fiber packing may be conveniently characterized at a number of different length scales is provided. New micrographic preparation techniques are presented, that allow microscopic characterization of uncured prepreg material. This provides the starting point for an analysis that is intended to uncover the links between processing sequence, micro-structural variation and attendant variability in structural performance. A computer code is presented that allows automatic characterization, in terms of fiber volume fraction maps, of micrographic images including those from previously published articles. A preliminary version of a finite element model that interrogates the effect of fiber packing on stress profiles and associated micro-cracking patterns is also presented.					
15. SUBJECT TERMS Composites, Prepreg, Microstructure, Characterization, Structural Performance					
16. SECURITY CLASSIFICATION OF:			17. LIMITATION OF ABSTRACT U	18. NUMBER OF PAGES 68	19a. NAME OF RESPONSIBLE PERSON Gregory P Dillon
a. REPORT U	b. ABSTRACT U	c. THIS PAGE U			19b. TELEPHONE NUMBER (Include area code) (814) 865 5879

Final Report

**Influence of Prepreg Microstructures on
Structural Performance of Polymer Matrix
Composites**

Principal Investigator: Dr. Gregory P Dillon

**Composite Materials Division
Applied Research Laboratory
The Pennsylvania State University
110 Technology Center
University Park, PA 16802**

For Period: 1 February 2002 to January 31 2005

Agreement Number: F49620-02-1-0098

ARL CMD Report Number AFOSR-GPD-7-15-2005

20050901 069

Table of Contents

	Page
List of Figures	iii
List of Tables	vi
1.0 Executive Summary	1
2.0 Program Objectives and Approach	6
3.0 Accomplishments/New Findings	8
3.1 Microstructural Analysis	8
3.1.1 Detailed Description of Matched Filter Automated Image Analysis Tool	31
3.1.2 Application of Automated Image Analysis to Micro-cracking	38
3.3 Finite Element Analysis	47
3.4 Statistical Analysis	58
4.0 Summary	61
5.0 References	62

List of Figures

Figure		Page
1	Conceptual Representation of Analysis Approach	7
2	Voronoi Cells Showing Different Fiber Volume Fractions and Clustering in Different Fiber Arrangements	9
3	Method for Determining Voronoi Cells (Dirichlet Tessellation)	9
4	Micrograph of IM7/977-2T Laminate Autoclave Cured at 350oF and under 100 psi plus Vacuum (Magnification = 50X)	10
5	Central Region of IM7/977-2T Laminate with Areas of High, Low and Intermediate Fiber Volume Fractions Labeled as AOI1, AOI2 and AOI3 Respectively (Magnification = 200X)	10
6	High Magnification Micrograph of AOI 1 Showing Circles and Polygons Used to Determine Fiber Volume Fraction	11
7	Dirichlet Tessellation of AOI 1	11
8	Dirichlet Tessellation of AOI 2	12
9	Dirichlet Tessellation of AOI 3	14
10	Microstructures Used to Evaluate Threshold Analysis as a Means of Determining Fiber Volume Fraction Variation (a) Manual Dirichlet Tessellation Method (b) Automated Threshold Method	15
11	Ply Thicknesses of Aligned Graphite Fiber Laminates Consolidated at Different Autoclave Pressures	16
12	Aligned Graphite Fiber Laminates Consolidated At 25psi Plus Vacuum, Showing Resin Rich Areas at Tow Boundaries	16
13	Aligned Graphite Fiber Laminates Consolidated at 5psi plus Vacuum, Showing Resin Rich and Fiber Rich Areas	17
14	Image of Graphite/Epoxy Laminate Central Ply with Threshold Set to Distinguish Fibers from Matrix Material	18
15	Variation of Threshold Value Necessary to Accurately Represent the Fiber Volume Fraction Variation (Drift)	19
16	Manual Image Analysis used to Determine Local Fiber Volume Fractions	19
17	Manully constructed Grid Used to Determine Local Fiber Volume fractions (a) Base Grid (b) Grid Showing Vf Data	20
18	Low Magnification View of Central Ply of (0/90) 2s Graphite Epoxy Laminate	20
19	Fiber Volume Fraction Variation in Central ply of (0/90)2s Laminate	21
20	Polished Prepreg Laminate Showing Large Variations in Fiber Packing Arrangements	22
21	Prepreg Material Showing Image Calibration Areas Used in Threshold Analysis	22
22	Comparison of Manual Fiber Volume Data with Threshold Values in Prepreg Image Calibration Areas	23
23	Fiber Volume Fraction Variation on Uncured Prepreg Material	24
24	Sample fiber extracted from a micrograph containing thousands of fibers	24

List of Figures (Contd')

Figure		Page
25	Sample pixels showing indexing method used in matched filtering	25
26	Sample fiber image and parent micrograph that will be scanned for fiber center determination	26
27	Three dimensional plot of matched filter function for the image shown in Figure 26	27
28	Matched filter function plot with original image	27
29	Section of uncured prepreg material and corresponding thresholded matched filter function	28
30	Close up of thresholded, matched filtered, closed image taken from Figure 29	28
31	Prepreg image with fiber center locations superimposed	29
32	Graphite/Epoxy laminate containing microcrack	29
33	Graphite/Epoxy laminate showing fiber centers and Voronoi cells	30
34	Fiber volume fraction plot for laminate shown in Figure 32	31
35	Fibercenter2 Graphic User Interface (GUI) displayed upon launching the automated image analysis tool	32
36	Imported image in the fibercenter program	32
37	Illustration of Polygon feature used to identify a region of interest (ROI) in image	33
38	Correlator statistic dialog box	33
39	Dialog box used to assign thresholds to a selected image	34
40	Generation of Voronoi cells in the image Region of Interest	35
41	Data saving options in the fibercenter2 program	36
42	Initial dialog box in the fvfplot program	37
43	Typical image output from fvfplot program	38
44	Central ply of a (0/90) ₂ S laminate tested to onset of microcracking	39
45	Fiber centers and associated Voronoi cells for laminate shown in Figure 44	39
46	Fiber volume fraction map for micro-cracked composite laminate made from YLA material	40
47	Fiber volume fraction map showing gradient plot across a selected horizontal line	40
48	Fiber volume fraction map for large fiber assembly with crack path highlighted	41
49	Scanned reproduction of micro-crack image published by Abry et.al in 2001	41
50	Scanned Voronoi cell analysis of image shown in Figure 49	42
51	Fiber volume fraction map and associated gradient plot for Abry et. al. image	42
52	Graphite Fiber Prepreg Mounted in Room Temperature Epoxy under 60 psi Pressure	44

List of Figures (Contd')

Figure		Page
53	Aligned Graphite Fiber Prepreg Material Mounted in Room Temperature Epoxy under 60 psi Pressure	44
54	Aligned Graphite Fiber Prepreg Material, Pressure Mounted and Free Standing, with Associated Thickness Profiles	45
55	Uncured Prepreg Material Mounted and Polished using a Two- Stage Process	45
56	Illustration of two stage mounting process used to produce micrographs from uncured prepreg	46
57	Deformation Contour of the Finite Element Grid Used to Represent a Generic Composite Microstructure	47
58	Internal Strain and Stress Contours for Regular Hexagonal Fiber Arrangements at Three Different Volume Fractions	48
59	Micrograph of Intermediate Level Fiber Packing Region and Associated Internal Strain and Stress Finite Element Models	48
60	Internal Strain Contours for Observed Fiber Arrangements in Areas of Interest (AOI's) 1, 2 and 3 of Carbon/Epoxy Laminate	49
61	Internal Strain Contours for Observed Fiber Arrangements in Areas of Interest (AOI's) 4, 5 and 9 of Carbon/Epoxy Laminate	50
62	Internal Strain Contours for Observed Fiber Arrangements in Areas of Interest (AOI's) 6, 7 and 8 of Carbon/Epoxy Laminate	51
63	Image of microcracked composite published by Lafarie – Frenot et. al. along with the associated Vornoi cell grid	52
64	Strain profile developed by horizontal axis stressing of the microstructure published by Lafarie - Frenot et. al. along with the corresponding fiber volume fraction map and selected gradient	52
65	Fiber Centers as Transferred to FEA Mesh Generator	53
66	Voronoi Cell Tessellation as Calculated by FEA Mesh Generator	54
67	Sample FEA Mesh, as Generated by Automated FEA Mesher	55
68	FEA Model, Predicted Strain, Uniform Edge Load at Right Side of Specimen	56
69	FEA Model, Predicted Stress, Uniform Edge Load at Right Side of Specimen	56
70	FEA Model, Predicted Displacement, Uniform Edge Load Applied at Right Side of Specimen	57
71	Cumulative Distribution Function and Probability Density Function data for Fiber Area Fraction in Sample Microstructure	58
72	Micrographs of uncured graphite epoxy prepreg material and laminate fabricated by conventional autoclave processing	59
73	Fiber volume fraction maps for uncured prepreg and laminate micrographs shown in Figure 72	59
74	Example of output from automated image analysis tool being used to generate statistical data	60

List of Tables

Table		Page
1	Voronoi Cell Fiber Volume Data for AOI 1	12
2	Voronoi Cell Fiber Volume Data for AOI 2	13
3	Voronoi Cell Fiber Volume Data for AOI 3	14

1.0 Executive Summary

This study provides methods by which composite prepreg materials can be characterized at the microscopic and higher levels. By applying established spatial tessellation schemes developed by Dirichlet, a means by which fiber packing may be conveniently characterized at a number of different length scales is provided. New micrographic preparation techniques are presented, that allow microscopic characterization of uncured prepreg material. This provides the starting point for an analysis that is intended to uncover the links between processing sequence, micro-structural variation and attendant variability in structural performance. A computer code is presented that allows automatic characterization, in terms of fiber volume fraction maps, of micrographic images including those from previously published articles.

A preliminary version of a finite element model (FEM) that interrogates the effect of fiber packing on stress profiles and associated micro-cracking patterns is also presented. This FEM was evolved from an initial form based on an ideal hexagonal packing grid to a more practical configuration in which fiber center data captured from real micrographs are used to form the basis of a Finite Element grid generated from the Dirichlet tessellation of the analyzed composite section plane. Initial results show very clearly the impact of fiber arrangements on the stress and strain profiles within real fiber networks. This approach to interrogation of effects of normal architectural variations on material response has been applied in a preliminary fashion to the particular problem of micro-crack development in composites subjected to transverse ply loading. Dedicated laminates, as well as legacy published material data, were used to provide preliminary insight into the influence of fiber packing on such strength based parameters. While no formal validated theory is offered based on this study, significant initial data suggest a relationship between micro-crack path development and fiber volume fraction gradients. While recognizing that any chosen material cross section is unlikely to coincide precisely with crack initiation locales, the common, though not uniform, tendency for crack development to follow regions of high fiber volume fraction gradient strongly suggests that crack propagation, and therefore critical strain energy release rates, is critically influenced by fiber arrangement.

The goal at the outset of this program was to provide an analytical tool, and associated experimentation methods, that could be used by the design community to accelerate the process of new material certification, particularly as applied to prepreg forms. By addressing the particular issue of fiber architecture variation, the relationship between process parameter variations (both in prepreg production and laminate fabrication) and resultant performance attributes were sought. A number of key developments were identified at the outset of the program that were thought critical to the successful development of the desired rapid transition capability. A self consistent variation characterization technique was required that could allow variability to be quantified at a number of different length scales. To a certain extent the Voronoi cell analysis (based on the Dirichlet tessellation) provided a ready made solution to this problem at program outset. However, while application of such techniques to 'model' fiber architectures had

been performed in a number of prior studies, practical methods suitable for analysis of real microstructures had not been developed. More fundamental to the development of the required 'cradle to grave' characterization of prepreg composite laminates, however, was the ability to capture the initial state of the material. Several potential micrographic techniques were assessed, but eventually a new two stage mounting and polishing technique was developed that allowed generation of requisite quality images from uncured prepreg material. This development, described in detail below, is considered an important achievement of the program.

Having identified a capable characterization methodology, significant early effort was devoted to applying the Dirichlet analysis to laminates processed under different conditions. YIA, Inc., as a fully capable prepreg manufacturer, provided material that was produced under optimal conditions, but also performed some production runs in which common defects (resin rich areas, dry fibers, missing tows etc.) were engineered into the material. These materials were also processed into laminates under different processing conditions in order to determine the effect of process variation on the development of architectural features that *may* impact performance. The early work on Dirichlet tessellation was performed manually. This effort, while time consuming and painstaking, provided useful information on basic material configurations and processing influences thereof. More importantly, however, it provided critical insights into how the process might be automated. At the outset, this was identified as another critical piece of the puzzle. Mid program efforts based on development of uniform sample preparation and photographic techniques were frustrated by the natural, and practically unavoidable, occurrence of exposure variations in conventional image processing. Promising initial results with thresholding approaches applied to color and gray scale images suggested that rapid analysis of large images could be conveniently effected by a method (described in following sections) based on local pixel calibration. However this was later abandoned in favor of an approach based on signal processing, where the pixel values comprising a sample fiber image were used to 'search' for similar entities in larger multi fiber (greater than 3,000) images. This technique was implemented with great success and a code was developed using the MATLAB platform that allowed rapid analysis of large fiber assemblies, with great tolerance for inferior image qualities. Examples of the use of the code in characterizing scanned copies of previously published data are given in this final report.

The final critical element of the desired analysis tool identified at program outset was a means of determining effects of architectural variations on measurable mechanical properties. It was decided early on that, while a number of micromechanical analysis theories exist for composites, the finite element method would be expected to provide the most convenient means of quickly characterizing structural parameter variations. Initially a simple approximation of observed microstructures was used, based on omission of fibers from an ideal hexagonal grid. This provided invaluable insight into the range of variational effects observed in real laminates. However, ultimate program focus yielded what is believed to be one of the more important contributions of the program. A Voronoi Cell Finite Element code has been developed that takes the output from the image analysis program described above and *automatically* generates a finite

element grid based on the tessellation. Grid generation based on Voronoi cells has been demonstrated before. However such programs have limited their analyses to relatively low fiber volume fractions and, as before, have generally been applied to simulated (rather than real) architectures. The integration of a powerful automated image analysis tool with an automated finite element analysis technique provides the foundational architecture of a rapid analysis method that that will allow variations in new and developing materials to be determined in the context of mechanical performance.

While providing much of what was sought at program outset, activity to date has not fully achieved the ambitious goals set forth in the proposal. A critical remaining task is to determine the large scale relationship (if any) between variation in laminate structural performance (as characterized by strength, stiffness etc.) and observed stochastic features in the microstructure. Pattern recognition and data mining techniques have been preliminarily applied, but this area remains as a significant challenge in the achievement of the overall program goals. At time of writing these issues are being studied in a follow-on program funded under the MEANS II initiative.

In summary, this program has succeeded in assembling the broad range of tools, methods and techniques needed to form an integrated approach to characterizing the effect of material variation on composite performance. Key barriers have been removed, including the limitation of micrographic analysis to solid cured laminates, the inability to automate image analysis of real microstructures and the lack of an automated finite element code capable of rapidly representing material architectures for mechanical analysis. Continuing program activity in MEANS II will apply these methods to the particular problem of micro-crack development (due to mechanical loading or resin degradation) in high temperature polymer matrix composites. However it will also focus on configuring the established capability into a broader analysis architecture that will constitute a tool that can be used in the design cycle to determine the impact of variability considered here on the suitability of emerging materials for structural high temperature applications.

As the performing center the Applied Research laboratory has brought a wide range of professional and academic competencies to bear on the program. Following is the required cumulative list of personnel who have contributed to this program, under the general functional headings in which they performed program tasks.

Program Management

Dr. Gregory P. Dillon – Research Engineer - Principal Investigator

Laminate Processing/Sample Preparation/Materialography

Eric Strauch – Associate Research Engineer – Laminate Process Engineering
Erik Takacs – Assistant Research Engineer – Materialography and Laminate Processing
Donald Stiver – Assistant Research Engineer – Sample Preparation
Barry Musser – Engineering Aide – Laminate Processing

Edward Good – Engineering Aide – Materialography
Christopher Rachau – Research Assistant - Laminate Preparation
Adam Roslund - Undergraduate Research Student – Sample Preparation

Materialographic Technique Development

Bryan Mayrides – Undergraduate Research Student – Prepreg Polishing Technique

Automated Image Analysis

James Ferlez - Undergraduate Research Student – MATLAB Code Development

Finite Element Analysis

Dr. Kevin Koudela – Research Associate, Head of Composite Materials Division – FEA Code Development

Dr. James Tarter – Research Associate – FEA Code Development; Automated Methods

Terri Merdes – Research Associate – Finite Element Analysis

Clark Moose – Research Assistant – Finite Element Analysis

John Pitterle – Research Engineer – Finite Element Analysis

This program, while providing support to three undergraduate research students did produce any research theses. However the follow on program will support a Ph.D student in Materials engineering. At time of writing the following publication has resulted from program research [1].

“Influence of Composite Microstructure on Structural Performance,” Gregory. P Dillon & Bryan D. Mayrides, SAMPE 35th Annual Technical Conference in Dayton, Ohio, September 28th to October 2nd, 2003.

A brief program plan for this project was presented at the Workshop on Durability, sponsored by the Defense Advanced Research Projects Agency and held in Woodland Hills, California on December 5-6, 2001. A similar, but somewhat more detailed, program plan was presented to the Accelerated Insertion of Materials Program personnel at Boeing, Canoga Park, California on Wednesday, December 5th, 2001.

The initial findings of this project were presented at the Air Force Office of Scientific Research Polymer Matrix Composites Program Review held at the Hyatt Regency, Long Beach California on Saturday May 18th, 2002. The presentation was entitled ‘Characterization of Variability in Prepreg Microstructures’ and detailed the initial efforts at standardizing an image analysis technique, based on Voronoi Cell Tessellation, that is used to characterize prepreg variability at various length scales. The presentation also covered initial efforts to represent the effects of prepreg variability on mechanical behavior, using a finite element analysis technique.

Early program findings were also presented at Aeromat 2002 Conference and Exposition in the Accelerated Insertion of Materials Session on Wednesday June 13, 2002 at the Rosen Plaza Hotel in Orlando Florida. The presentation was given under the program title and, in addition to the topics covered at the Polymer Matrix Composites Program Review, also outlined initial efforts to develop a technique to examine uncured prepreg microstructures. In addition the talk covered an expanded finite element analysis of laminate microstructures that showed the effect of observed variation in material architecture on responses to applied loads.

Interaction with the DARPA Accelerated Insertion of Materials (AIM) program, continued throughout the program. ARL/PSU participated in the AIM Principal Investigator's workshop from March 19-21, 2003 in Santa Fe, New Mexico.

ARL/PSU was also a participant in the MEANS theme program review workshop in Boulder, Colorado from August 6th to 8th, 2003. Aside from the progress update ARL/PSU also provided input in a materials modeling focus group, and later drafted further input for the working group summary paper for submission to AFOSR program leadership.

Two additional publications are currently in draft form. These include a paper describing the two stage sample preparation technique used to capture uncured prepreg microstructures, and a further article on the automated image analysis code development described in this report. Publications are expected to occur in late 2005.

2.0 Program Objective and Approach

The exhaustive 'material allowable' development process traditionally required to build confidence in the structural design community has hampered rapid insertion of emerging materials into defense platforms. The effects of application specific parameters, such as temperature, moisture exposure and cyclic loading conditions are determined by similarly time consuming methods, with the result that 'lab-to-platform' implementation times are sometimes on the order of 20 to 30 years, with associated costs in the tens of millions of dollars. In order to circumvent this time consuming and costly material qualification process, methods are required to accurately predict effects of processing history on composite microstructure variations. As with all engineering materials, variations in microstructure have an impact on structural performance and associated reliability. Local variations in fiber structures add to chemical or compositional variations in the matrix resins to create a situation where significant resultant structural variations may be difficult to classify or analyze. While many studies have focused on the influence of microstructure variations on prepreg properties, no definitive studies have been completed that analyze impact on structural behavior. *Therefore, the objective of the proposed program is to develop an analysis tool that will accurately predict the effects of variations in prepreg materials on structural performance.* This tool will also allow the impact of such variations on the expected scatter in test data to be accurately determined. In its final form, this analysis tool could be incorporated into Boeing's AIM-C program for prepreg characterization and could be used to determine the expected performance of new prepreg materials based on simple measures of microstructure and processing characteristics without having to develop an exhaustive 'material allowable' database.

To successfully accomplish the objective the following sub tasks were identified at the start of the program

1. Fully characterize variations in advanced prepreg materials in terms fiber spacing, tow spacing, fiber waviness, occurrence of common defects and fiber volume fractions.
2. Determine the influence of prepreg production parameters and composite material characteristics (fibers, resins, fiber sizings, tows sizes) on the occurrence of such variations.
3. Determine effects of common composite production methods (principally lay-up and autoclave cure) on prepreg structure variations.
4. Apply established and evolving analysis techniques to determine the effects of architectural variations on strength and stiffness-based design data for advanced polymer matrix composites.
5. Determine the contribution of characterized variations on observed scatter in mechanical test data.
6. Devise intelligent experimental techniques that allow efficient capture of structural data and preclude exhaustive allowables database development.
7. Ultimately develop an analysis tool that provides a predictive link between observed microstructure variations and structural behavior, with particular emphasis on performance variability.

In order to execute the goals of program, a team was established with expertise in micro- and macro-mechanical analysis of composite materials and structures, prepregging and processing of composites, stochastic and variational analysis of test data, non destructive and destructive evaluation, and specialized test technique development. The team consisted of the Applied Research Laboratory at The Pennsylvania State University (ARL/PSU) and YLA, Inc. ARL/PSU has historically been the preeminent source for design, analysis and test of structures and systems for Navy surface and undersea programs. Project personnel also had significant experience in insertion of composites into aerospace and other industrial applications. YLA, Inc. specializes in custom prepreg development, and has a dedicated research facility uniquely equipped to carry out the type of parametric investigation of process parameter variation that is fundamental to this investigation. In addition YLA has installed unique on-line monitoring capability that allows real time detection of prepreg product variability.

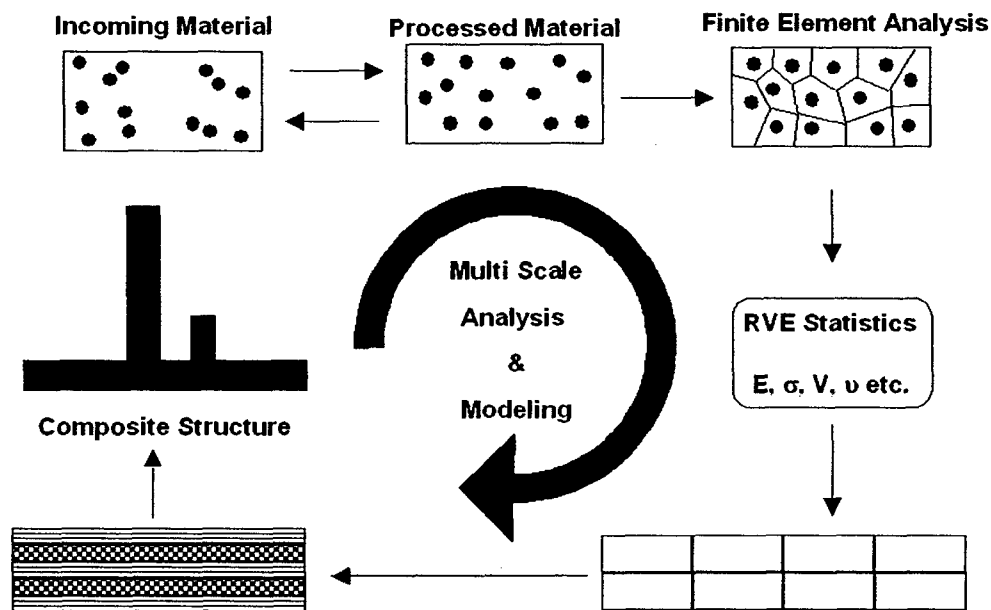


Figure 1 Conceptual Representation of Analysis Approach

The basic structure of the analysis approach adopted in the program is illustrated in Figure 1. Several key elements are depicted. Incoming prepreg material possesses some state of microstructural order, determined by the parameters of the prepregging process. This material is then processed in some way, conventionally by hand lay-up and autoclave cure. The processing stresses impact the original state of order, principally by forcing the fibers to assume closer packing arrangements, and, perhaps secondarily, by conferring thermally dependant chemical character in the resin and interface. Significant effort was devoted to determining the structure of the 'starting material' and the quantifiable microstructural characteristics that can be used to track the evolution of the structure as it passes through the fabrication process.

Once the microstructure is 'locked' in place, efficient material and structural analysis techniques are necessary to determine realistic variability metrics. A key challenge that was addressed in great depth was to determine the size and characteristics of a representative volume element within which the variability of key material parameters is captured and represented at an appropriate length scale. Voronoi cell analysis has proven valuable in determining local fiber volume fraction variations. *However, the precise scale at which the analysis should be applied remains unknown, and will be a primary focus of ongoing work.*

With a realistic representation of local variability, standard variational numerical techniques can then be applied to determine the impact of material variability on structural performance. Verification of modeling must rely heavily on 'scale-matched' experimentation, where predictions of response variability can be tested at the length scale at which the observation is made.

3.0 Accomplishments/New Findings

The principal accomplishments in this program were in three main areas;

- Microstructural analysis
- Prepreg and Laminate Microscopy and Characterization
- Finite Element Analysis

The following sections describe the evolution of novel techniques used to provide data to characterize the prepreg composite variability effects that were the primary focus of this program. It must be noted at the outset, however, that the rather ambitious goals that were set out were not fully achieved in this program. However, as a summarizing statement, it can reasonably be claimed that the critical elements of the desired analysis tool were successfully assembled, and at time of writing, follow on work seeks to leverage these developments to complete the initially identified task.

3.1 Microstructural Analysis

Development of an automated microstructure analysis technique was considered crucial to the success of the program. Such a technique would form a foundation for multi scale modeling of composite structures and would also provide the quantitative link between material variability and structural performance.

A number of image analysis techniques have been applied to composites and sophisticated software programs have been developed. Automated techniques that allow critical fiber arrangement parameters to be captured have not been developed, however. Voronoi cell tessellation has been shown, in a number of prior programs, to be a useful means of determining, among other parameters, local (on the fiber level) fiber volume fraction variations. This is the necessary starting point for a statistical treatment. Some early work on technique development in this program was focused on application of Voronoi methods to composite microstructures. Figure 2 shows a schematic

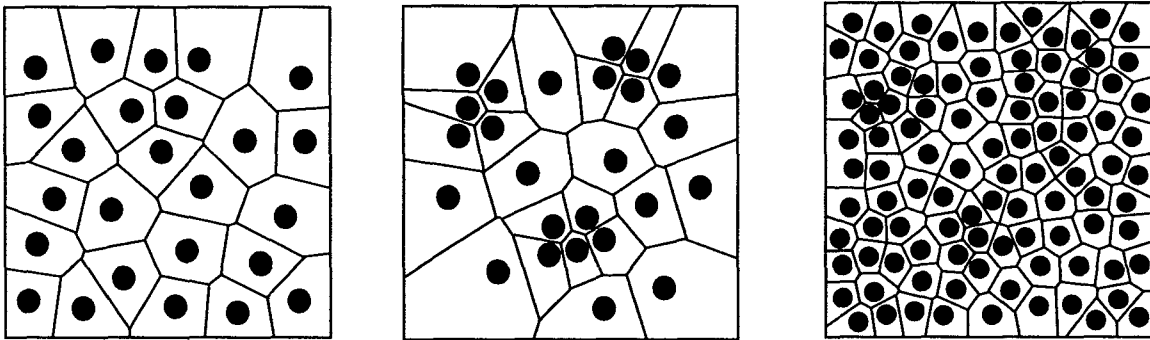


Figure 2 Voronoi Cells Showing Different Fiber Volume Fractions and Clustering in Different Fiber Arrangements

representation of the application of this technique to a number of typical microstructures. Essentially, this tessellation scheme allows a region of matrix material to be associated with a given fiber. The simple method used to achieve this spatial tessellation, also known as a Dirichlet tessellation, is shown in Figure 3. The significance of the method is that for each fiber center location a surrounding associated area is defined such that all points within that area are closer to the fiber center than to any other fiber center. Once the Voronoi cell has been defined in this way the local, fiber level, fiber volume fraction can be calculated by simply dividing the fiber cross sectional area by the area of the associated cell.

The utility of this technique was initially evaluated using the IM7/977-2T autoclave cured laminate shown at 50 times magnification in Figure 4. The micrograph shows the general

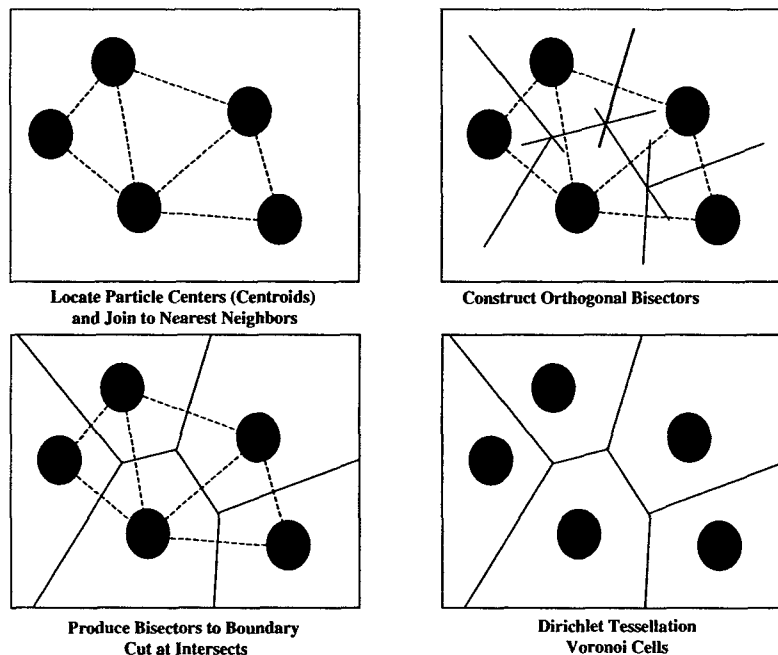


Figure 3 Method for Determining Voronoi Cells (Dirichlet Tessellation)

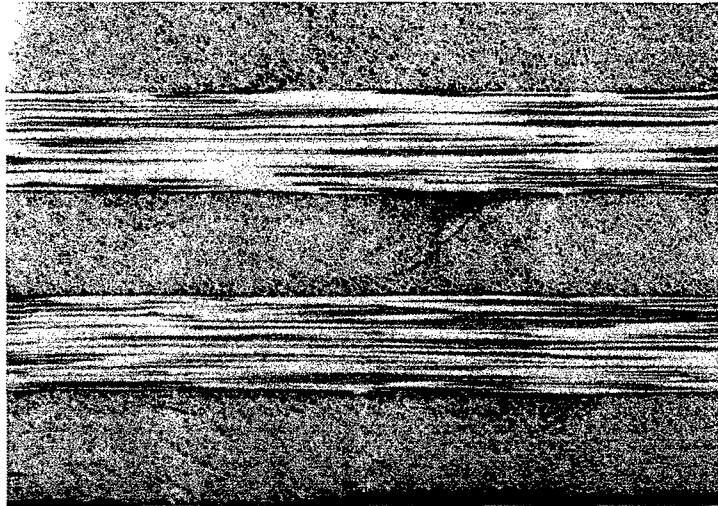


Figure 4 Micrograph of IM7/977-2T Laminate Autoclave Cured at 350°F and Under 100 psi plus Vacuum (Magnification = 50X).

high quality, low void content character of the laminate. A central area of the laminate was chosen for application of the Dirichlet analysis. This area, shown in Figure 5, was chosen because it contained, within a relatively small space, regions that had distinctly different fiber packing arrangements. The area labeled AOI 1 (denoting Area of Interest 1) shows a relatively high fiber volume fraction, while AOI 2 and AOI 3 are areas of low and intermediate fiber volume respectively. The area designated AOI 1 is shown at an effective magnification of 3,000X in Figure 6. Polaroid micrograph images were scanned and imported into a commercial version of the Image Program developed by National Institutes of Health. The Image software was first used to determine the fiber volume fraction of AOI 1 as a basis for comparison to the Dirichlet tessellation calculated fiber volume. Circles were drawn to represent the fiber perimeters and these are labeled as

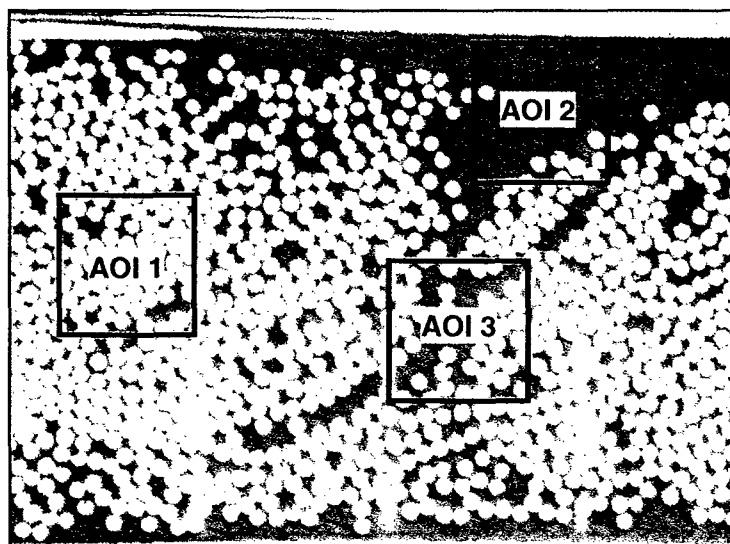


Figure 5 Central Region of IM7/977-2T Laminate with Areas of High, Low and Intermediate Fiber Volume Fractions Labeled as AOI1, AOI2 and AOI3 Respectively (Magnification = 200X)

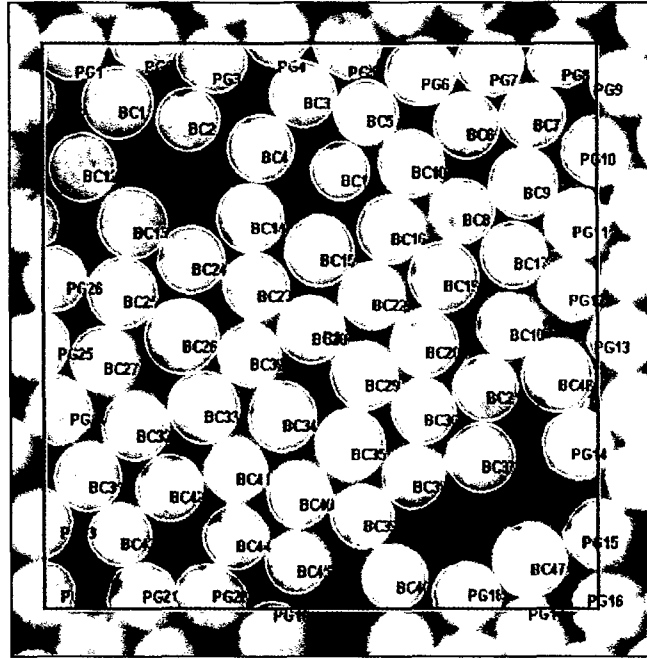


Figure 6 High Magnification Micrograph of AOI 1 Showing Circles and Polygons Used to Determine Fiber Volume Fraction

BC1 through BC48 in Figure 6. The polygon tool of the software program was used to define the perimeters of fibers that did not lie fully within the border of the selected area of interest. These are identified as PG1 to PG28 in Figure 6. The image calibration feature of the program allowed accurate measurements to be taken, and this tool was used to evaluate the diameters of the fibers contained in AOI 1. The average fiber diameter thus calculated was $5.04 \mu\text{m}$ with a standard deviation of $0.25 \mu\text{m}$, which correlates well with

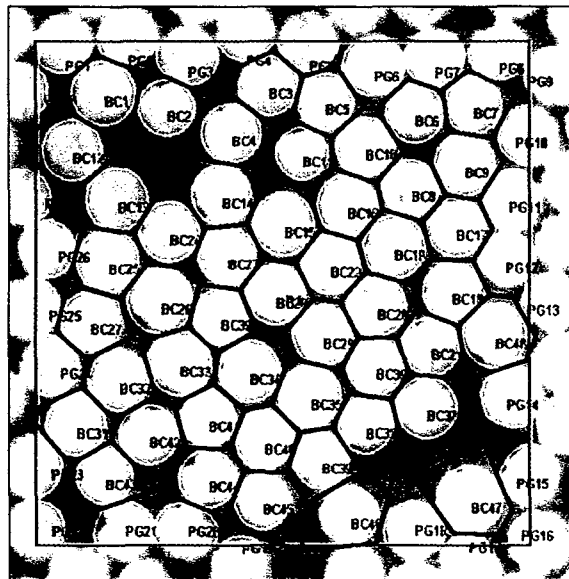


Figure 7 Dirichlet Tessellation of AOI 1

data published by the manufacturers for these AS4 fibers. By summing the areas of the circles and polygons and dividing by the total area of the box the fiber volume fraction for this area of interest was determined to be 67.54%. This is considered well within the range of typical high quality aerospace composite laminates or structures.

The Dirichlet tessellation method was applied to AOI 1 and the result is shown in Figure 7. The method is applied only to fibers that are fully contained within this area of interest. Note that this procedure was done 'manually'. Considerable program effort, described in detail below was devoted to automating this task. Based on the tessellation, local fiber

Table 1 Voronoi Cell Fiber Volume Data for AOI 1

BC1	67.56	BC13	53.32	BC25	72.68	BC37	46.45
BC2	48.22	BC14	58.19	BC26	76.08	BC38	56.04
BC3	71.92	BC15	68.63	BC27	68.51	BC39	67.37
BC4	59.87	BC16	73.40	BC28	70.92	BC40	69.23
BC5	71.15	BC17	75.95	BC29	73.26	BC41	71.39
BC6	71.25	BC18	69.99	BC30	74.37	BC42	64.47
BC7	73.83	BC19	75.80	BC31	72.74	BC43	61.78
BC8	74.97	BC20	71.03	BC32	67.79	BC44	64.69
BC9	77.48	BC21	75.88	BC33	76.23	BC45	47.04
BC10	73.58	BC22	76.98	BC34	70.66	BC46	51.87
BC11	55.94	BC23	72.58	BC35	74.62	BC47	55.22
BC12	60.89	BC24	70.15	BC36	77.43	BC48	72.13

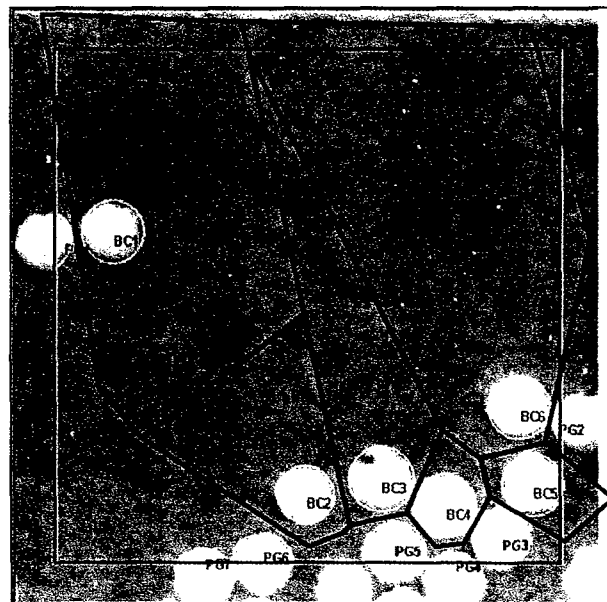


Figure 8 Dirichlet Tessellation of AOI 2

volume fractions were calculated for each Voronoi cell corresponding to the circles used to calculate the AOI fiber volume fraction. The results are shown in Table 1. The data illustrate the wide variations in fiber volume fractions that occur within a very small area. The average fiber volume fraction of all cells was 67.74%, compared to 67.54% calculated using the Image Program software. However, the local cell volume fractions varied from 46.45% all the way up 77.48%. Note that the theoretical maximum, corresponding to hexagonal close packing, is 90.7%. It is worth pointing out that in all of the microstructures examined in the program not a single region of perfectly ideal packing was identified. The Dirichlet tessellation of an ideally packed fiber arrangement would yield an array of regular hexagons. The variation of fiber volume fractions calculated is significant. Structures consisting of 46% and 77% fiber volume composite laminates would have dramatically different properties. However one of the major challenges facing this program was to determine the length scale at which variations in fiber volume have an impact on structural behavior.

Identical analysis procedures to those outlined above were applied to AOIs 2 and 3. A high magnification view of AOI 2 is shown in Figure 8. Average fiber diameter (5.23 μm) and associated standard deviation (0.22 μm) are again within published ranges whereas the fiber volume of the area is very low, at 10.13%. The Voronoi cells for this microstructure are also shown in Figure 8. One of the disadvantages of the technique is illustrated in this area. It is questionable that the matrix material contained within the cell enclosing BC6 is realistically 'associated' with the identified fiber in any way. It is certainly true that this fiber is not reinforcing the entirety of the matrix material contained within the cell. One utility of the tessellation scheme was that it provided a natural means of developing a finite element grid to represent a given microstructure (described later. However it may not be useful in determining how resin rich areas of the kind shown in Figure 8 should be analyzed.

Table 2 Voronoi Cell Fiber Volume Data for AOI 2

BC1	4.14
BC2	10.67
BC3	11.87
BC4	50.22
BC5	41.82
BC6	3.20

The Voronoi Cell fiber volume data for AOI 2 are shown Table 2. In this case it is not surprising that the average Voronoi cell volume fraction (20.32%) does not correspond with that calculated for the full area of interest. Again there is a large variation in volume

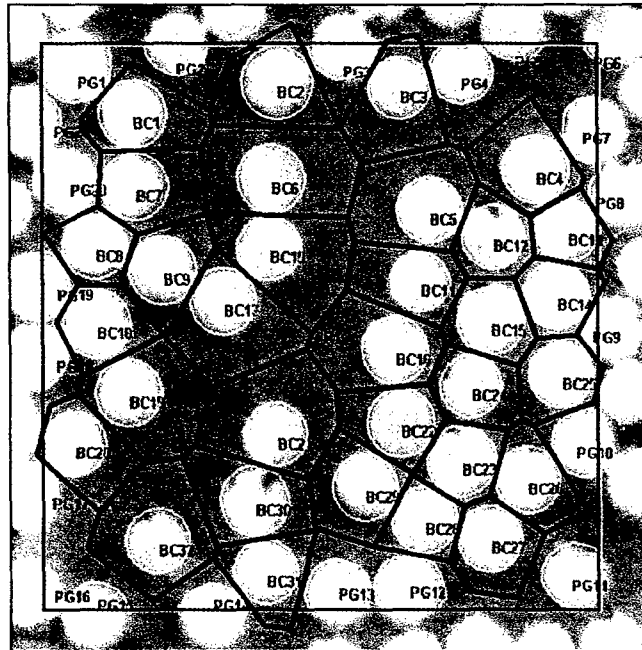


Figure 9 Dirichlet Tessellation of AOI 3

fraction, ranging from 4.14% to 50.22%. Interestingly, however, this variation is not much greater than that calculated for the relatively highly fiber loaded AOI 1.

A high magnification view of AOI 3 is shown in Figure 9. Again average fiber diameter (5.02 μm) and standard deviation (0.21 μm) data are well within published ranges. The fiber volume of the area would be characterized as intermediate, at 45.88%. The Voronoi cells for this microstructure are also shown in the figure. The association of matrix material with given fibers is more realistic in this microstructure, though again there is a wide variation in fiber volumes as evidenced in Table 3. In fact the range of values

Table 3 Voronoi Cell Fiber Volume Data for AOI 3

BC1	47.74	BC9	53.25	BC17	29.65	BC25	55.36
BC2	46.80	BC10	26.98	BC18	57.50	BC26	52.75
BC3	34.27	BC11	36.67	BC19	30.81	BC27	47.84
BC4	41.96	BC12	54.77	BC20	45.62	BC28	68.79
BC5	30.58	BC13	62.54	BC21	24.24	BC29	42.61
BC6	26.18	BC14	64.92	BC22	55.28	BC30	42.48
BC7	43.87	BC15	57.59	BC23	68.80	BC31	51.16
BC8	63.61	BC16	34.61	BC24	50.18	BC32	26.12

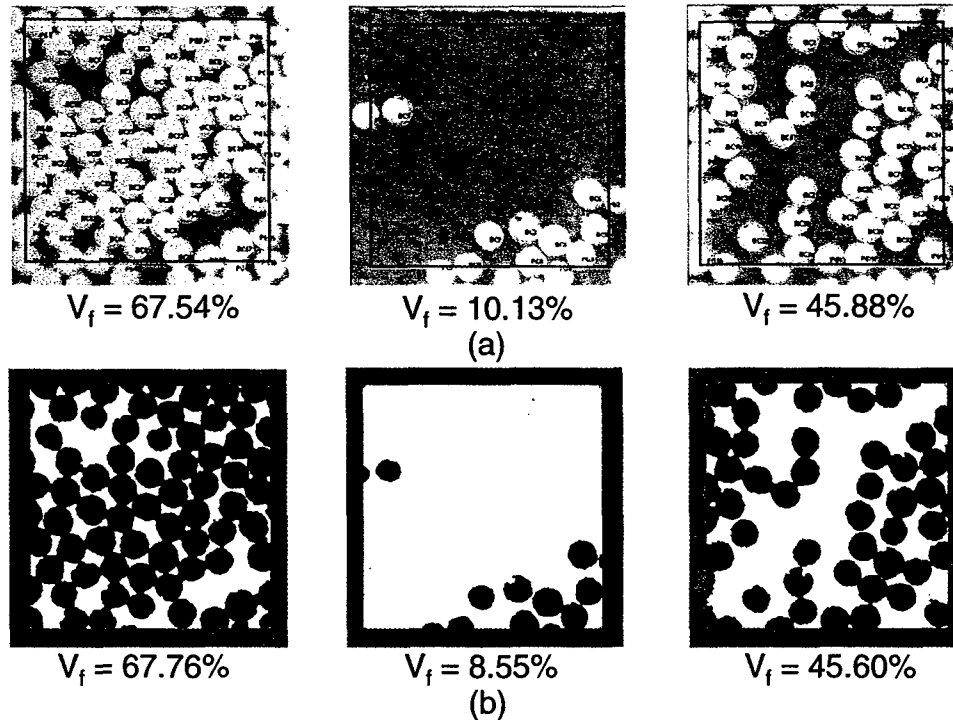


Figure 10 Microstructures Used to Evaluate Threshold Analysis as a Means of Determining Fiber Volume Fraction Variation (a) Manual Dirichlet Tessellation Method (b) Automated Threshold Method

(24.24% to 68.8%) is nearly identical to that noted for the very low volume fraction AOI 2. This is a very intriguing result and opens up the possibility that at some stage in the prepreg production process the relationship between the maximum fiber volume fraction and the minimum fiber volume fraction within a given area is somehow locked in. Interestingly, this agrees with a principal analytical finding presented by Gutowski [2] who showed that for a wide range of consolidation curves determined by several research teams there was a unique relationship between the fiber volume fraction at which the fiber network began to carry measurable load and the final volume fraction attained after full consolidation. This, and other such theories, have important implications for the present study, as they may eventually provide a potential link between processing sequence and variability within a given fiber architecture.

The image analysis techniques outlined above have proved useful in representing and analyzing detailed features of composite microstructures. However an automated scheme for conducting these analyses was sought in order to provide a tool with practical analytical value. The first effort at developing a rapid volume fraction mapping technique was based on a pixel threshold analysis approach. Using image scanning software packages, such as SigmaScan applied in this project, pixel values are set to some threshold value, such that all pixels below are switched to white and all those above set to black (or some other desired color). Standard images are presented as being composed from 256 colors or gray scale levels. Therefore an intermediate value can be used to highlight some desired microstructural entity such as a fiber.

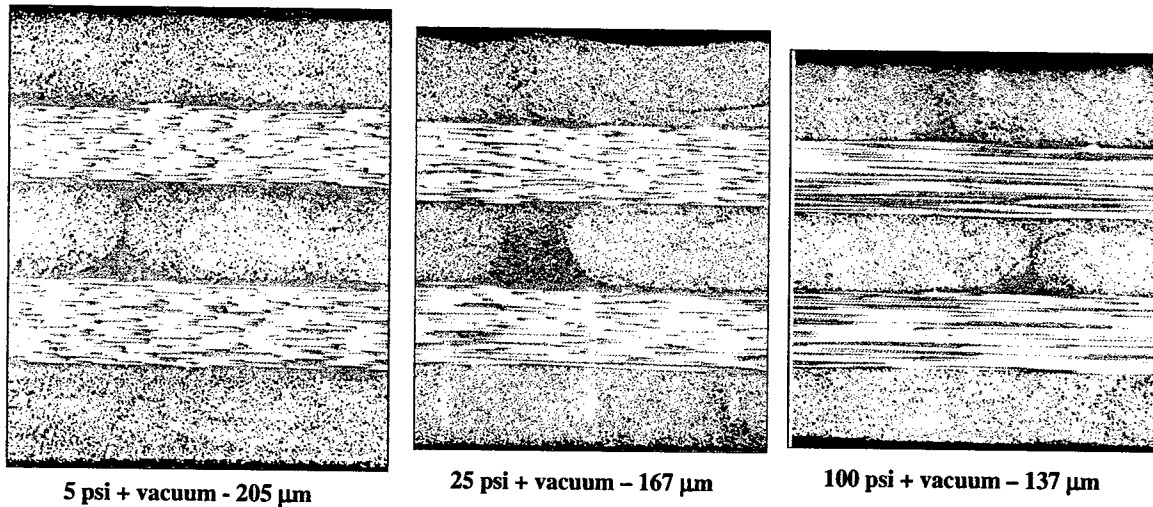


Figure 11 Ply Thicknesses of Aligned Graphite Fiber Laminates Consolidated at Different Autoclave Pressures

Figure 10 shows the microstructures analyzed within the selected areas of interest, with the associated fiber volume fractions calculated using the method of circles and polygons detailed above. Using a gray scale image with a pixel threshold value of 112 the fiber volume of AOI 1 was determined to be 67.76%. The same threshold value was then used to determine the corresponding fiber volume data for AOIs 2 and 3. As can be seen in the Figure 10b, the values yielded are very close to those calculated using the circles and

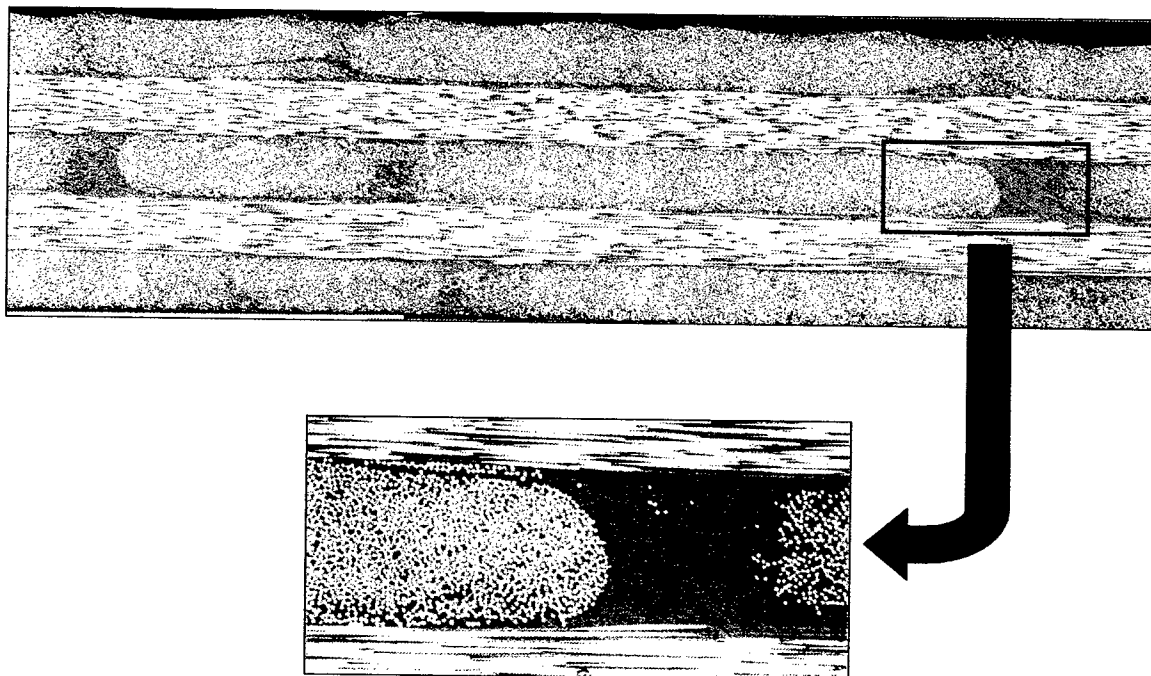


Figure 12 Aligned Graphite Fiber Laminates Consolidated At 25psi Plus Vacuum, Showing Resin Rich Areas At Tow Boundaries

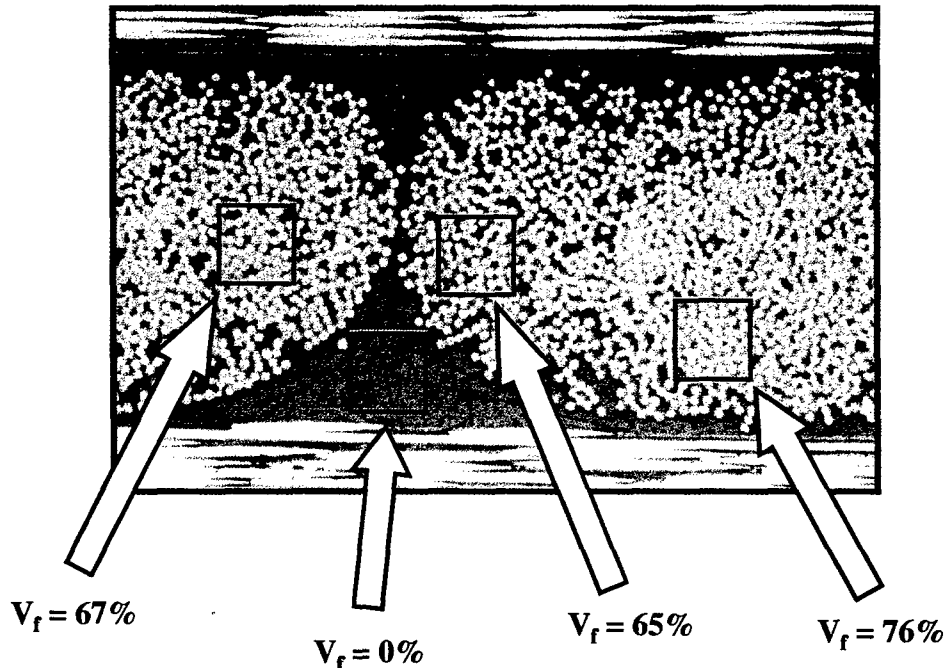


Figure 13 Aligned Graphite Fiber Laminates Consolidated at 5psi plus Vacuum, Showing Resin Rich and Fiber Rich Areas

polygons method. It was believed that this technique would allow enormous amounts of fiber volume variation data to be collected at a wide range of length scales, provided that a standardized image preparation technique can be applied. This would necessarily mean that all micrographs be obtained under identical and repeatable lighting conditions, and that image scanning and display parameters be consistent. A point image calibration scheme would also be necessary to ensure that salient microstructural entities, principally fibers, resins and voids, be displayed with reference to some recognized calibrated gray scale before application of the threshold analysis. Obviously, standardized grinding and polishing processes must precede all such image capture and analysis procedures. A series of experiments was conducted in this that was designed to gain an initial insight into the rearrangement of fiber architectures accruing from various processing cycles. Figure 11 shows AS4/977-2T laminates that were processed at the same cure temperature (350°F) but at different autoclave pressures. The variation in laminate consolidation is evident from the noted differences in ply thickness.

Closer examination reveals the trend toward elimination of the usual resin rich layer at ply boundaries as pressure is increased. It is interesting to note that, even at a very low consolidation pressure of 25 psi plus vacuum, a high quality laminate, essentially free of voids and bubbles, results.

Figure 12 shows the laminate that was consolidated at 25 psi plus vacuum. This micrograph was generated by 'stitching' together several adjacent images of the sample cross-section. Among the salient features are the relatively large resin rich areas that are remnants of the prepreg manufacturing process. Prepregs are made by laying together aligned fiber tows, which may contain anything from 3,000 fibers (3K tow) up to 100,000 fibers or more. Pressures generated at the nip rolls spread out the tows, but identifiable

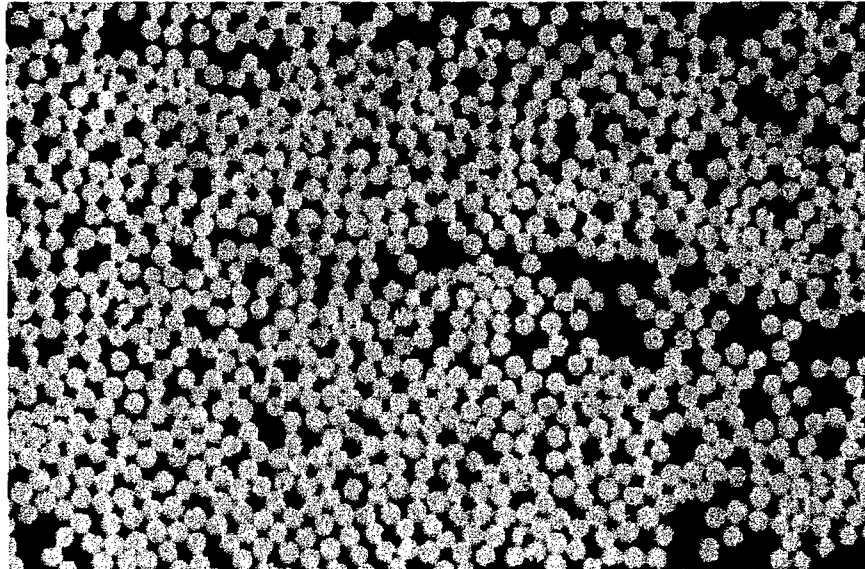


Figure 14 Image of Graphite/Epoxy Laminate Central Ply with Threshold Set to Distinguish Fibers from Matrix Material

gaps frequently remain, particularly as highlighted and magnified in the figure. It is evident from the images in Figure 11 that the laminate pressurization occurring during autoclave cure causes significant fiber rearrangement or 'healing' of flaws in the laminate. Capturing this fiber arrangement in the unprocessed prepreg material and tracking the restructuring that occurs in response to processing stresses was a key challenge of this program and is described in a later section of this report.

Figure 13 shows a cross section of the laminate that was processed using a 5 psi consolidation pressure with particular areas of interest highlighted as before. The local fiber volume fractions of these areas were evaluated using the threshold method, again using a cut-off pixel value of 112. This region is interesting for a number of reasons. It shows a relatively large resin rich area where no fibers are present. However immediately adjacent to this area locations are found in which the fiber packing is very dense. This suggests that the process of laminate consolidation is therefore one in which already high fiber volume fraction regions are forced together, essentially by an extensional flow process. While not particularly surprising, this does emphasize once more that capturing the prepreg microstructure is crucial to understanding the nature of variability in advanced composite materials.

The early focus of the microstructural analysis task described above was on the application of the Dirichlet tessellation technique to yield the Voronoi cell parameters for various microstructures prepared from graphite/epoxy prepreg. The technique constitutes a very useful means of determining local fiber volume fraction variations, and also provides a very convenient means of computing many parameters that may yet prove useful for classifying microstructural variation and relating it to stochastic features of mechanical test data. However, the focus was then shifted to developing techniques that can be applied on a larger scale. The underlying rationale is that meso-scale analysis techniques will allow rapid recognition of variations over relatively long length scales,

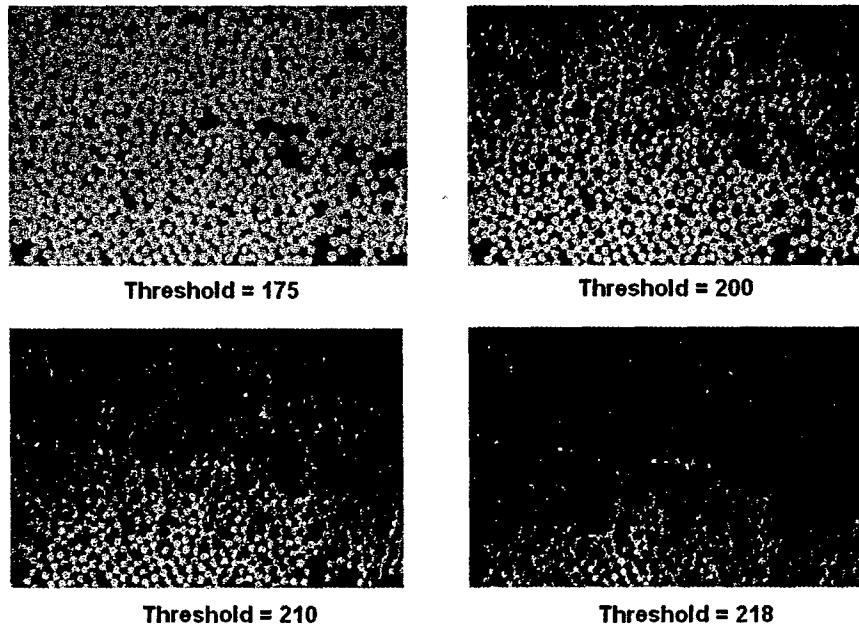


Figure 15 Variation of Threshold Value Necessary to Accurately Represent the Fiber Volume Fraction Variation (Drift)

which will guide the application of the micro-scale analysis techniques. Allied with the Finite Element Method, this was intended to identify an appropriate representative volume element, the microstructural variation of which can be determined by application of the Dirichlet method.

The most convenient method of determining fiber volume fraction variation over relatively large areas is by application of the 'threshold' technique mentioned above. The application of the technique is shown in Figure 14. A central area of the middle ply of a $(0/90)_{2S}$ laminate is shown with the matrix material set to appear as red. While the selected threshold level of 175 appears to accurately represent the relative amounts of fiber and resin present, further examination of the image highlights a problem

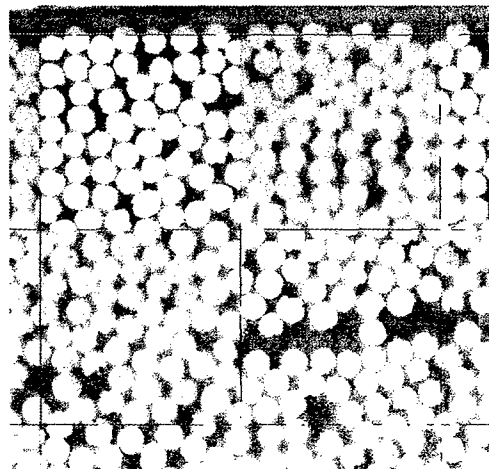


Figure 16 Manual Image Analysis used to Determine Local Fiber Volume Fractions

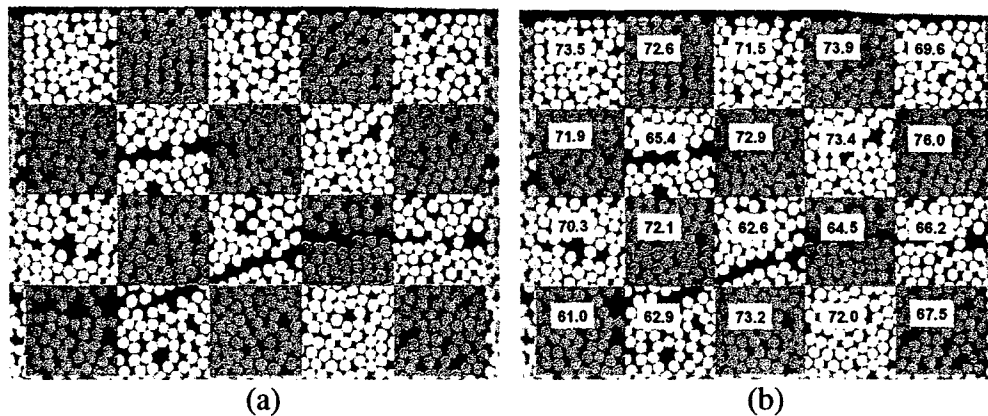


Figure 17 Manully constructed Grid Used to Determine Local Fiber Volume fractions (a) Base Grid (b) Grid Showing Vf Data

encountered repeatedly in the analysis of composite microstructures in this program. Figure 15 shows the same image examined with increasing threshold levels. The drifting phenomenon depicted is believed to be a result of very small differences in the lighting and scanning conditions, and perhaps even polishing effects in the preparation of the micrographs. The program did successfully generate a micrograph in which this nuisance feature was effectively suppressed. It should be noted that the same problem has been seen on a number of metal micrographs.

In order to devise a method of quantifying this effect, a more detailed analysis of the microstructure was undertaken. Figure 16 shows a close-up of an intermediate step in a manual process in which each fiber, within the nominally 50 fiber bundles, is highlighted in order to determine local fiber volume fractions. The complete image treatment is shown in Figure 17 (a) with relevant fiber volume data shown in Figure 17 (b). Interestingly the threshold values required to provide accurate local fiber volume fractions scaled almost exactly linearly along the direction of the drift shown in Figure 15. This was true in virtually all of the micrographs examined, though some more complex relationships were seen, particularly in micrographs taken at lower magnifications, e.g. 50x. This does suggest that a pixel calibration process could be applied to allow rapid analysis of images. In such an approach, real time adjustment of

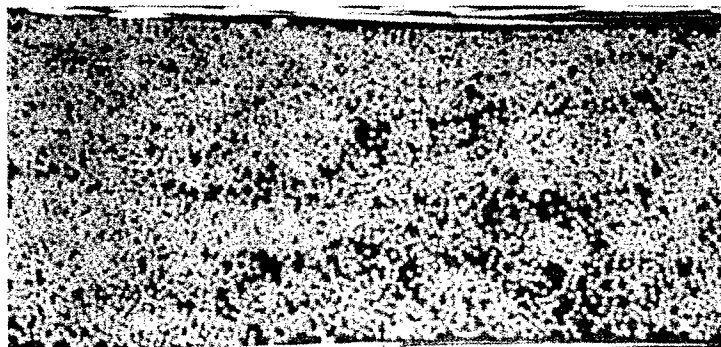


Figure 18 Low Magnification View of Central Ply of (0/90) 2s Graphite Epoxy Laminate

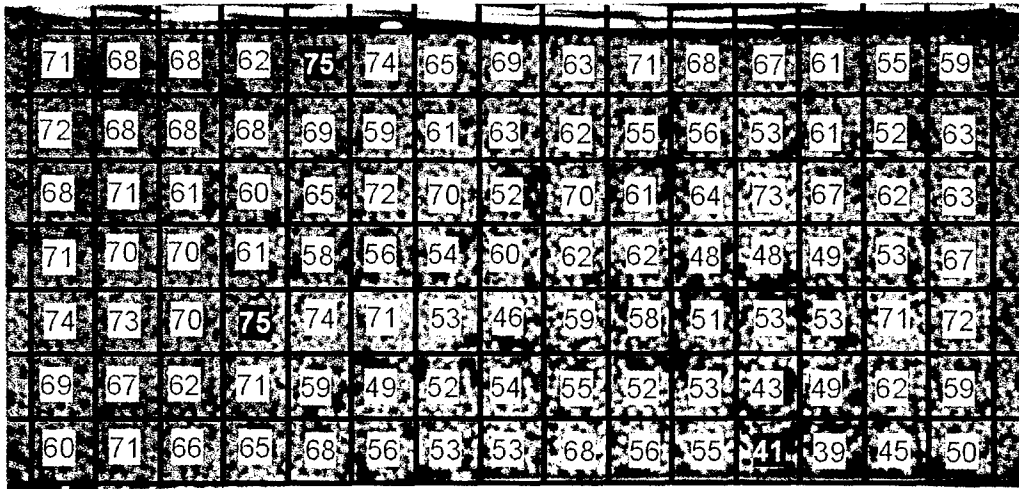


Figure 19 Fiber Volume Fraction Variation in Central ply of (0/90)_{2s} Laminate

threshold images would identify the direction of drift or 'texture' of the image. Local fiber volume fractions could be precisely determined in strategic locations. Then, finally, the pixel data could be adjusted over the entire image based on the texture analysis.

A manual version of the above procedure was applied on a larger area of the (0/90)_{2s} laminate. A general view of the area is shown in Figure 18. In some ways the information that is sought is visually evident in the picture. From a withdrawn perspective the brighter areas are easily identifiable as those in which the fiber volume fraction is higher. However, the variation of fiber volume fraction over this area is depicted, based on an adjusted threshold analysis, in Figure 19. Dividing the examined area into elements containing nominally fifty fibers or so, the variation in fiber volume for the prepreg ply is presented. As was the case with consideration of Voronoi data for cells on the same size order as those depicted, there is a very wide variation in fiber volume fraction. Oddly this variation (from 41% to 75%) is in a similar range to that seen in the Voronoi cells previously examined. Perhaps this points to some fractal character in sub ply fiber volume data, but more likely it shows that the fifty fiber cell may not be large enough to capture the variability of the fiber network as a whole. The threshold analysis was applied on cells at different length scales and statistical tests will be applied in follow on work to determine the appropriate scale of the analysis. The ultimate goal will be to use data of the type shown in Figure 19 to determine the appropriate representative volume element for a structural analysis, and to use the data from a Voronoi data treatment to determine the realistic variation in the properties of the individual elements.

These techniques were also used to examine the features of microstructures prepared from uncured prepreg materials (see micrographic preparation technique in following section.) A low magnification view of such a microstructure is shown in Figure 20. This is typical of the microstructures examined for the YLA prepreg material. Three

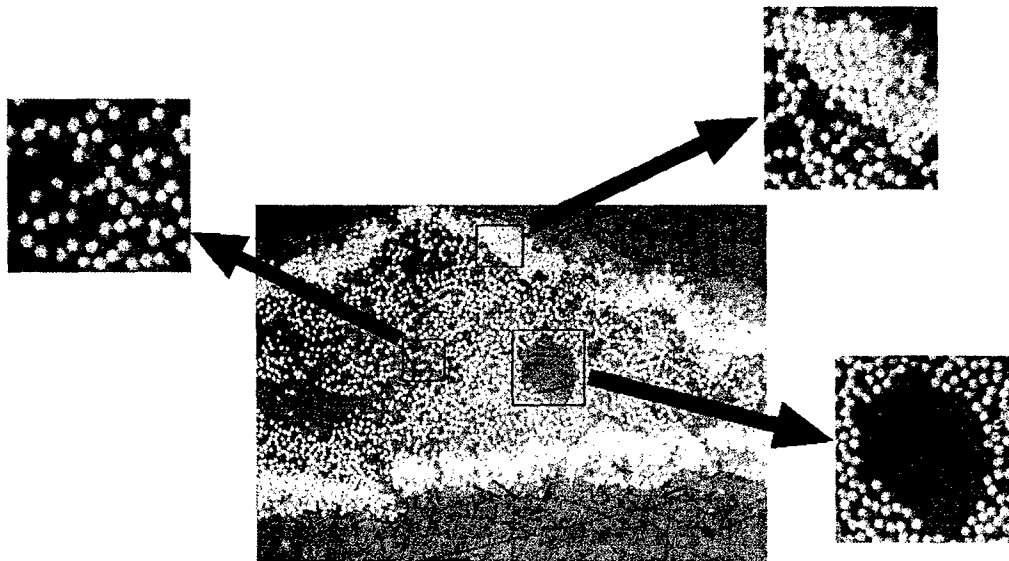


Figure 20 Polished Prepreg Laminate Showing Large Variations in Fiber Packing Arrangements

distinct areas are seen as highlighted by the surrounding higher magnification views. In general areas are seen in which no fibers are present. Before application of the two stage mounting technique (described below) it is suspected that this region was essentially a void, in which the fibers of the prepreg had moved apart. A disperse central region in which fiber packing is sparse, is also seen. However the most surprising feature is the tendency to high fiber packing at the edge of the ply. This was frequently seen in a number of microstructures, and is a feature of prepreg materials not believed to have been previously reported. The mechanism by which this occurs is open to speculation, but may be a result of the high tension applied to prepreg tows during the prepregging process. In such a process the outside fibers may be expected to pick up the majority of the load, since the uncured prepreg material would not be capable of carrying a shear stress. Therefore the inner fibers may have a mechanism available to them that allows

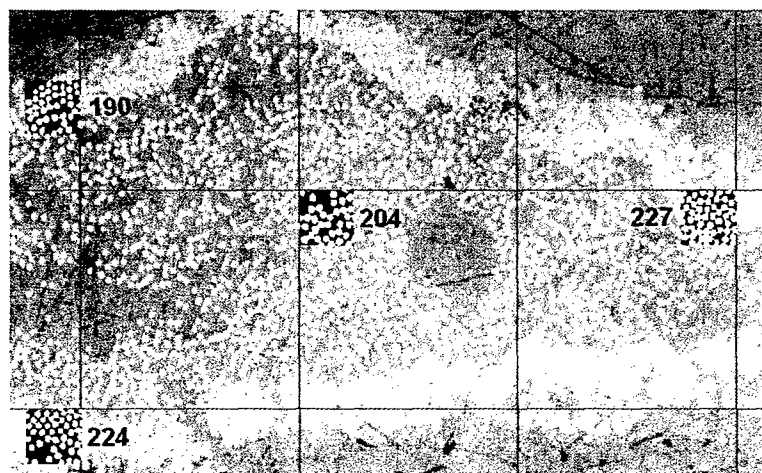


Figure 21 Prepreg Material Showing Image Calibration Areas Used in Threshold Analysis

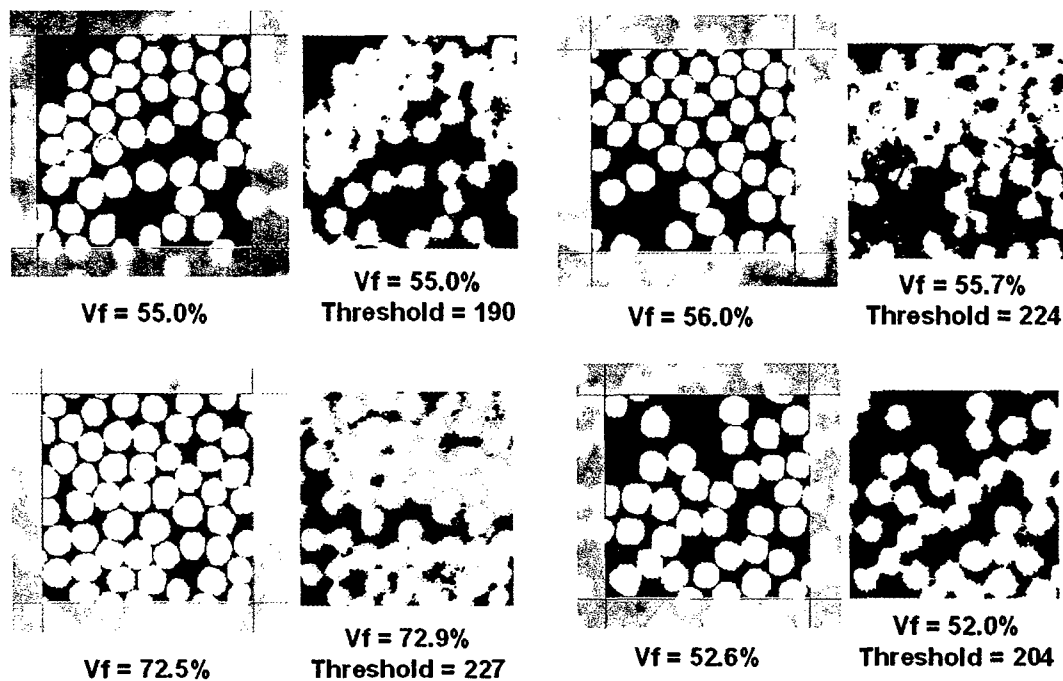


Figure 22 Comparison of Manual Fiber Volume Data with Threshold Values in Prepreg Image Calibration Areas

some degree of relaxation. The outer fibers are pulled tight and therefore forced to high fiber volume fractions. When the load is released (after spooling of the prepreg) the higher fiber volume fraction fibers may relax, pulling the inner fibers along with them to a lower fiber volume fraction. Whatever mechanism is responsible for this starting structure, it is a clear indication that the prepregging process has a strong influence on the composite architecture. A key challenge for this program was to determine whether this, or any other structural phenomenon uncovered in the study, exerts influence on the ultimate performance of the material. It is conceivable that a different fiber gripping mechanism applied in the prepregging process might lead to more even tensioning of the fibers and perhaps consequently less variation in the fiber distribution in the uncured material.

Application of the threshold analysis showed that the drift phenomenon occurred along a diagonal path (from the top left). Therefore the areas, or cells, highlighted in Figure 21 were selected for more detailed fiber volume fraction analysis. The results are shown in Figure 22, beside the corresponding threshold images (with the threshold values also shown in Figure 21.) It is evident from Figure 22 that further work needs to be focused on producing micrographs in which the natural contrast between the fibers and matrix is sharper. While all commercial image analysis packages allow contrast values to be manipulated, with some custom filters available, little can be done to achieve adequate delineation if the original image does not provide it. Different sample lighting

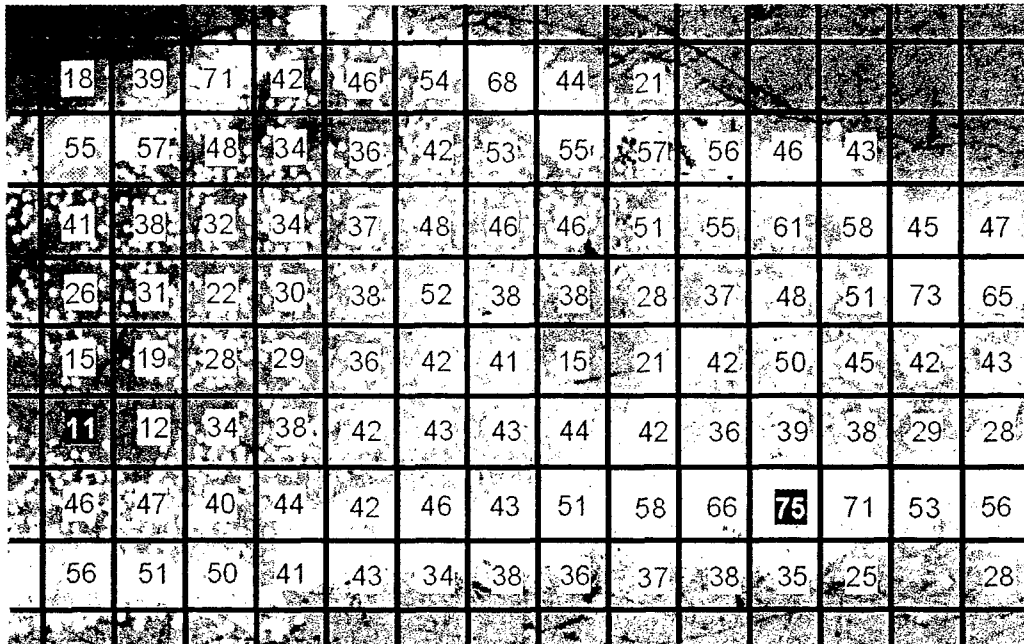


Figure 23 Fiber Volume Fraction Variation on Uncured Prepreg Material

approaches and perhaps some matrix staining or etching techniques that will allow fibers to stand proud above the background resin may prove fruitful.

Figure 23 shows the fiber volume fraction data for the uncured prepreg material. The 'calibration' cells are highlighted in the image along with the highest and lowest values of fiber volume fraction. It is interesting to note that areas exist in the prepreg material in which the fiber packing is just as dense as in the most tightly packed areas of the *cured* material. However there are areas in which the fiber volume fraction is very low, and movement of the grid might have yielded cells where the value was zero. *This further illustrates the need to determine the link between the microstructure of the starting material and the resulting finished part architecture.*

The threshold technique, described above, provides a means by which large areas of

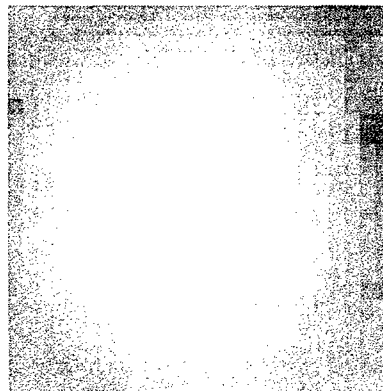


Figure 24 Sample fiber extracted from a micrograph containing thousands of fibers.

micrographic data may be analyzed. However automation of this technique, while feasible, was not achieved in this work. Therefore the method was de-emphasized in the later stages of the program in favor of an approach based on signal processing and analysis. This new technique, referred to as matched filtering, allows a typical fiber image to be captured and treated as a signal, essentially composed of its pixel values. This signal is then used to scan a larger image containing many fibers, and where a high correlation between the fiber signal and scanned image is found a candidate fiber center is identified. Simple image operators are then applied to discard smaller incidental entities, like scratches and inclusions, and the result is a very accurate fiber center array. This can then be conveniently operated on to determine packing parameters based on Dirichlet tessellations or any other technique of interest.

Approaches based on thresholding described above seek to determine whether a given pixel belongs to a fiber or not. The key shortcoming of single pixel intensity thresholding is that information from *neighboring* pixels, that can be used to greatly improve the ability to accurately classify the pixel of interest, is neglected. The notion of shape, which is important in this classification is lost to algorithms that threshold based on a single pixel value. Matched filtering seeks to determine whether a given pixel is a fiber center based on its immediate neighbors. In this paradigm a function that maps a neighborhood around and including the pixel of interest to a *single* real number is used, which then becomes the quantity that is thresholded.

The *Matched Filtering* technique is applied in problems where a *known* signal (in this case the pixels corresponding to a fiber) happens at an *unknown* point in space and with possible noise corruption. These conditions match very well the circumstances of the current problem, *if* the shape characteristics of the fiber are known. However the fact that fibers are relatively easily recognized in a given microstructure (by the human eye) and they are remarkably similar in size and shape can be exploited. It was mentioned above that, in the case of IM-7 fibers, the diameter was about $5 \mu\text{m} \pm 0.2 \mu\text{m}$.

The matched filtering technique begins with the selection of a 'sample' fiber. Figure 24 shows a typical fiber selected from a composite microstructure. Seen at a large magnification, the distinct boundary between fiber and matrix material is not as clearly evident as in the parent image.

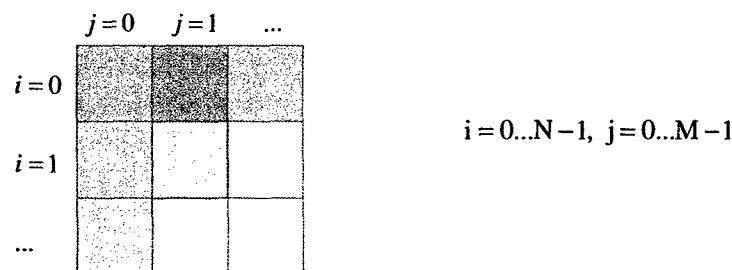


Figure 25 Sample pixels showing indexing method used in matched filtering.

In the *Matched Filtering* problem, the example signal that is selected actually defines an $f(\cdot)$, or a function that maps the pixel values to a real scalar $\gamma (\in \mathfrak{R})$. Let $x_{i,j}$ represent the samples from the neighborhood (*which has the pixel of interest at its center*) and $w_{i,j}$ represent the samples from the example indexed, as shown in Figure 25.

Define the quantities;

$$\bar{x} = \frac{\sum_{i=0}^{N-1} \sum_{j=0}^{M-1} x_{i,j}}{N \cdot M} \quad \bar{w} = \frac{\sum_{i=0}^{N-1} \sum_{j=0}^{M-1} w_{i,j}}{N \cdot M}$$

In these circumstances the matched filter function is given by,

$$g(x) = \frac{\sum_{i=0}^{N-1} \sum_{j=0}^{M-1} (x_{i,j} - \bar{x})(w_{i,j} - \bar{w})}{\left\{ \sum_{i=0}^{N-1} \sum_{j=0}^{M-1} (x_{i,j} - \bar{x})^2 \right\}^{1/2} \cdot \left\{ \sum_{i=0}^{N-1} \sum_{j=0}^{M-1} (w_{i,j} - \bar{w})^2 \right\}^{1/2}}$$

This function, though apparently complex, can be interpreted in the following way; when x contains a centered fiber, $g(x)$ is large. Unfortunately, this necessitates a slight reexamination of how pixels are classified. Since $g(x)$ is large when x contains a centered fiber, the critical determination reduces to deciding whether or not the pixel of interest *represents the center of a fiber*. Thus, the best result is that (small) clusters of nearby points are identified that can be classified as fiber centers so that an average can be calculated to determine an actual pixel estimate for the fiber center.

An example of the application of the matched filtering technique is shown in Figure 26.

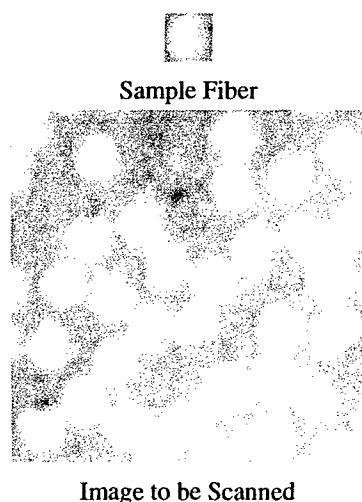


Figure 26 Sample fiber image and parent micrograph that will be scanned for fiber center determination

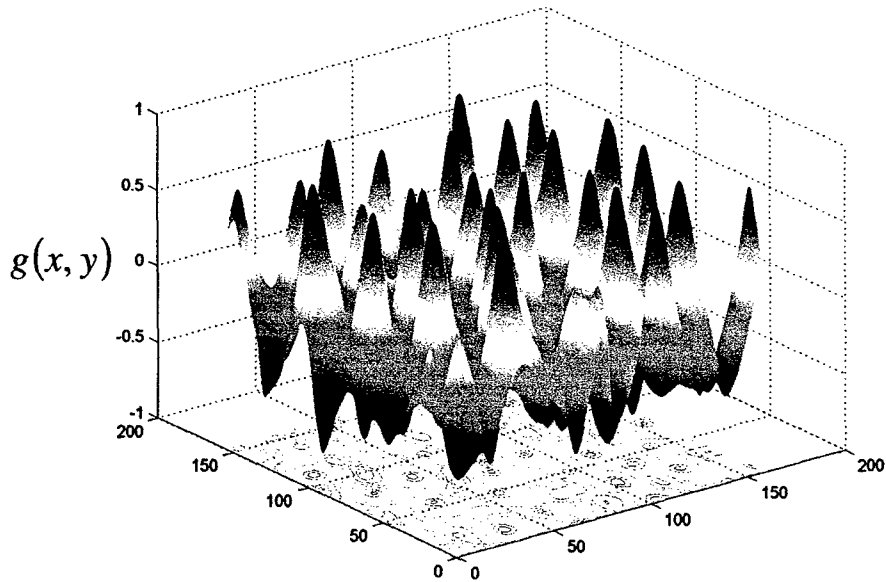


Figure 27 Three dimensional plot of matched filter function for the image shown in Figure 26

Note that the sample fiber was not extracted from this image but from a similar micrograph of a neighboring region. The matched filter function is calculated for every pixel in the image and the results are given in the three dimensional plot shown in Figure 27. The results show defined peaks that are *candidate* fiber centers. It might seem logical that evaluation of local maxima would allow reliable determination of fiber centers. However local maxima may also be associated with other microstructural entities that are not fibers, such as inclusions, small voids or bubbles in the resin. Therefore further 'clean-up' operations must be applied. However when the plot of the $g(x)$ function is shown beside the original image, as in Figure 28, it is evident that a capable algorithm for fiber center determination has been developed.

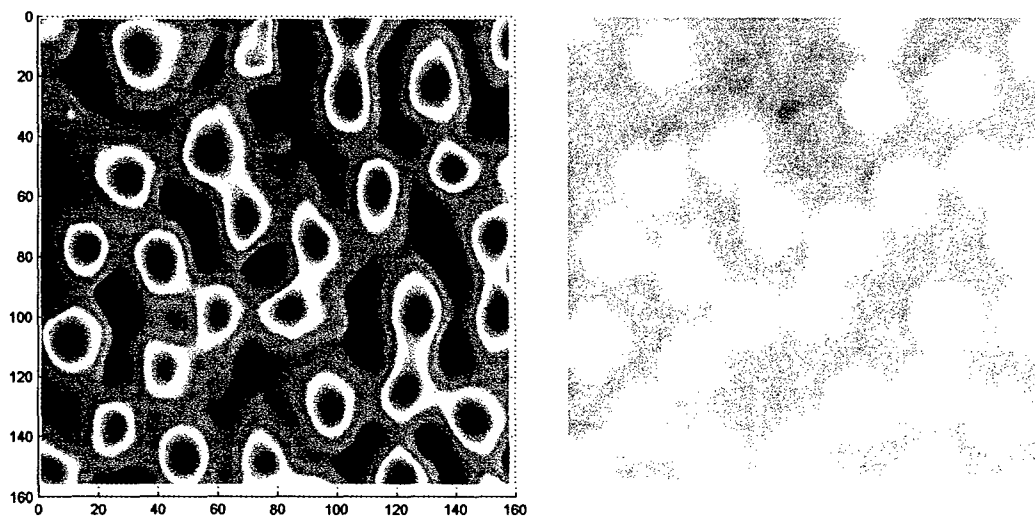


Figure 28 Matched filter function plot with original image

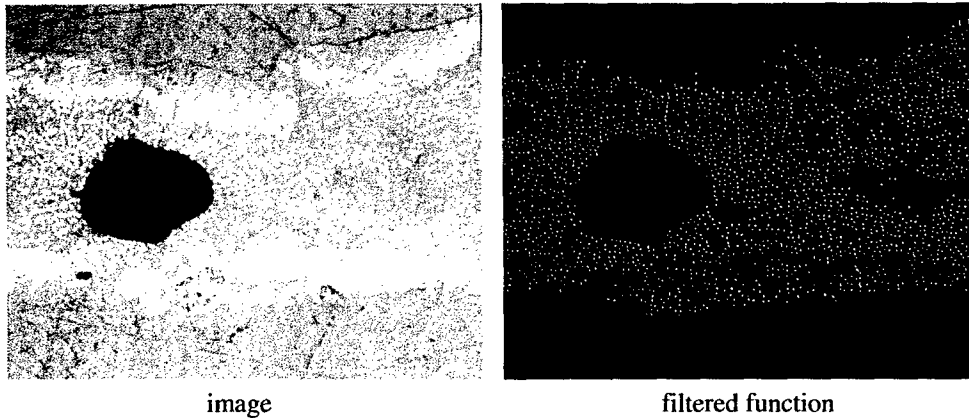


Figure 29 Section of uncured prepreg material and corresponding thresholded matched filter function.

The next step in the process is to threshold the matched filter plot. The matched filtering technique has essentially allowed the identification of entities that are much more clearly delineated from one another. In other words, the inherent problem presented by a high fiber packing array has been overcome. The distinctions between fibers are more clearly defined. Therefore the application of a simple thresholding technique will now yield a clearer distinction among fiber center and non fiber center *regions*.

In Figure 29 the thresholding of a matched filter plot is applied to a much larger image, in this case a section of uncured prepreg material. The original image is also shown for comparison. A close up of one section of this image is shown in Figure 30. The final step in the process is to conduct a simple image analysis procedure called 'closing' in which the threshold is adjusted in order to make the smaller (lower local peak correlation function) areas disappear. The remaining entities are then grown back to original size by an 'opening' process. The fiber centers are then determined by finding the centroids of the remaining particles.

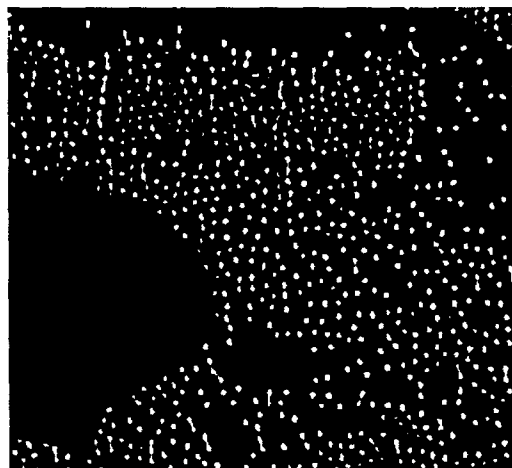


Figure 30 Close up of thresholded, matched filtered, closed image taken from Figure 29

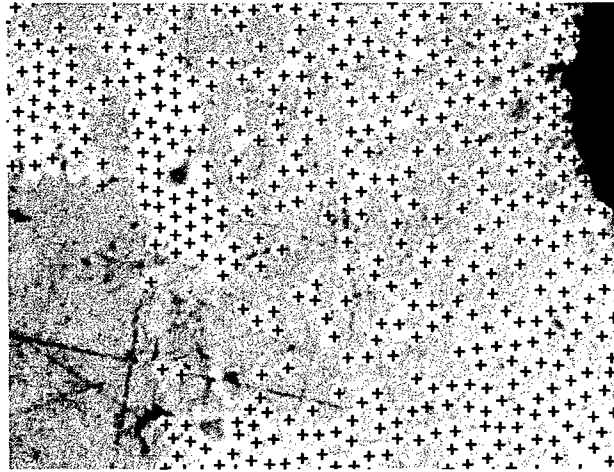


Figure 31 Prepreg image with fiber center locations superimposed

Note that the final latter steps in the process (closing, centroid determination) are common embedded functions in commercially available image analysis software packages. The final result is shown in Figure 31. The accuracy of the technique is very good, though it is not infallible. As can be seen in the figure, occasional pairs of fibers are mistaken for a single filament and some fibers are missed by the scan. However, as illustrated by the scratches in the image, the quality of sample preparation was, in this case, not optimal. These images were purposefully selected for application of the technique, under the assumption that if a high degree of accuracy could be demonstrated here a robust analysis tool would result. From the results shown above, this seems to be the case.

The full spectrum of capabilities of this new automated tool is illustrated in the following examples. Fiber center data such as those presented in the previous pages are useful in characterizing the fiber volume fraction variations in composites. In the concluding period of this program this tool was applied intensively to uncured and cured prepreg laminates in order to determine the effects of processing sequence on fiber architecture

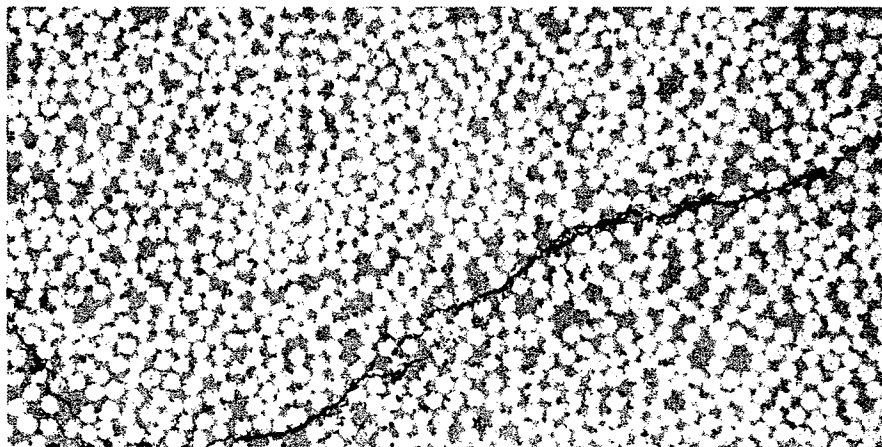


Figure 32 Graphite/Epoxy laminate containing microcrack

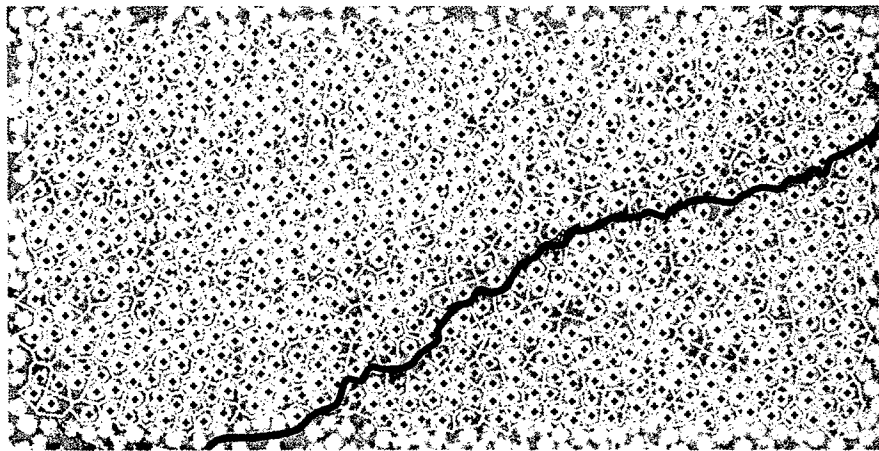


Figure 33 Graphite/Epoxy laminate showing fiber centers and Voronoi cells

and resultant impact on performance. In a following section the effects of fiber packing on crack propagation are explored. However an example of this type of analysis is presented here in order to illustrate the features of the analysis tool. Figure 32 shows a graphite fiber/epoxy laminate (fabricated ARL/PSU) that was loaded in bending to the point of crack initiation. The crack can be seen clearly running in a diagonal direction. Figure 33 shows the same laminate with the fiber centers having been located using the matched filtering technique. The figure also shows the Voronoi cells for the microstructure. Note that within the selected area the accuracy of the analysis is 100%. This supports the contention made earlier that the tool would operate very reliably on high quality micrographic images.

The tool automatically stores fiber center data in an x-y data file along with the associated Voronoi cell area data. By careful calibration of the image dimensions the average fiber radius is determined and this is then used to calculate the fiber volume fraction for each Voronoi cell. All of this data can be made available to other programs for statistical or structural analysis. In early program activity the methodology was developed by manual image analysis. However, by way of comparison, the image capture, analysis and Voronoi cell calculations for an image comparable to that in Figure 32 would take about 2 man days. With this new automated analysis tool the entire procedure can be completed in less than thirty minutes including about eight minutes of matched filter calculations on a Pentium 4, 1.4 GHz personal computer (assuming 1,000 x 1,000 pixels in the source image).

The final, and perhaps most important, feature of the program is that it allows fiber volume fractions to be plotted for any given microstructure. The result for the microstructure shown in Figures 32 and 33 is given in Figure 34. The original crack path is highlighted by a black line and seems to show that cracks follow paths of high fiber volume fraction gradient. This was the subject of finite element analysis and will be covered in more detail in the later sections. The tool allows the intervals of fiber volume fraction, shown in Figure 34 to be adjusted in whatever manner is desired. From a finite

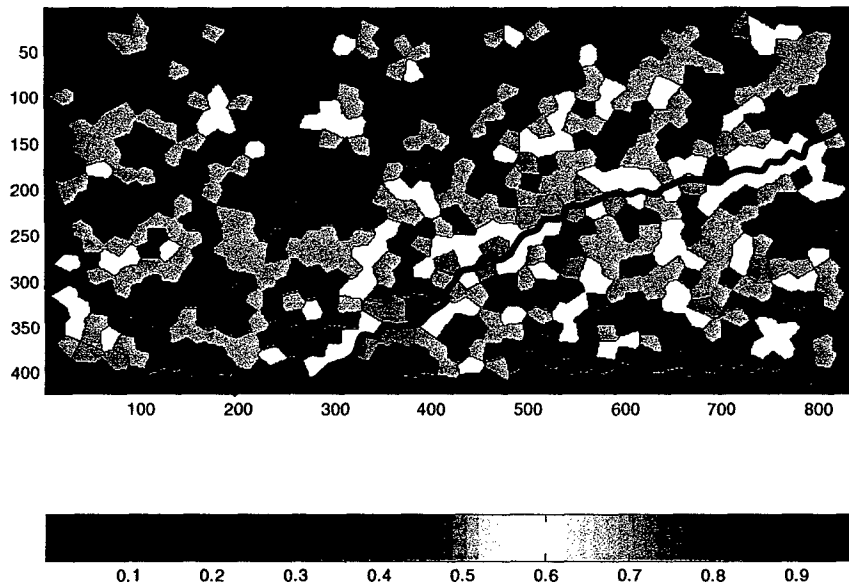


Figure 34 Fiber volume fraction plot for laminate shown in Figure 32

element modeling perspective this capability has important implications. Finite element analyses can now be performed based on material properties associated with particular ranges of fiber volume fraction, and this potentially will allow the critical scale of analysis necessary to capture variability effects to be determined. As stated previously this was a principal objective of the program at the outset, and significant effort will be devoted to completing this sub-task in the follow on program.

3.1.1 Detailed Description of Matched Filter Automated Image Analysis Tool

This section describes in detail the step by step use of the Automated Image Analysis Tool outlined in the previous section. The tool was developed using the MATLAB 7.0 computer code and a copy of the programs used is included with this report. At time of writing the program is capable of analyzing relatively large (on the order of 10,000 fibers) images in very short time frames. However, some code clean-up work is required to prevent the occurrence of error codes that are, for the most part, insignificant and do not generally lead to program crashes. However this code cleanup exercise will be completed in the follow on MEANS II program. The program is divided into two separate MATLAB codes; **fibercenter2**, which automatically detects fiber centers in scanned micrographic images and allows the Voronoi cells for the image to be computed, and **fvfplot** which allows the fiber volume fractions to be calculated based on fiber diameter data and the computed areas of the Voronoi cells. It should be pointed out that the Dirichlet tessellation, which yields the Voronoi cells, is an included subroutine within the MATLAB architecture. Therefore a code line that calls up this function is all that is necessary to complete this step. To use the automated image analysis tool the folders containing the above programs (**fibercenter2** and **fvfplot**) are placed in the MATLAB workspace. The **fibercenter2** program is then launched and the initial dialog box appears as shown in Figure 35. The 'open' command is then selected from the 'file' drag down menu and this opens a browser that is used to navigate to image files that maybe

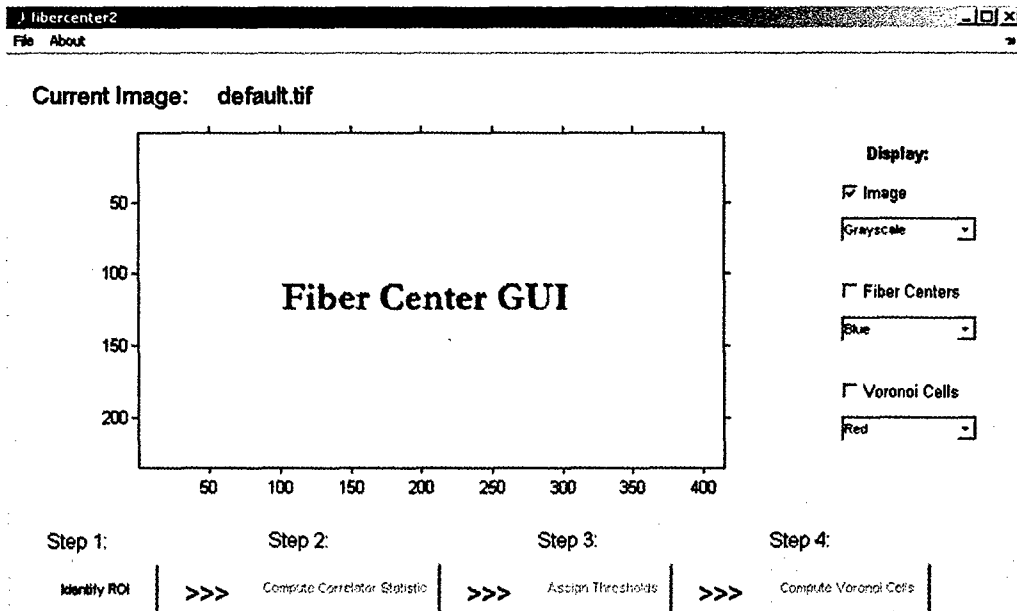


Figure 35 Fibercenter2 Graphic User Interface (GUI) displayed upon launching the automated image analysis tool

analyzed. When an image has been imported as shown in Figure 36 (the program is currently configured to analyze TIFF, JPEG and Bitmap formats) an area of interest is selected by clicking on the box beneath STEP 1. At this stage the optional displays (image, fiber centers and Voronoi cells) are selected by clicking on the check boxes on the right hand side and limited color options can be selected using the associated drag down boxes.

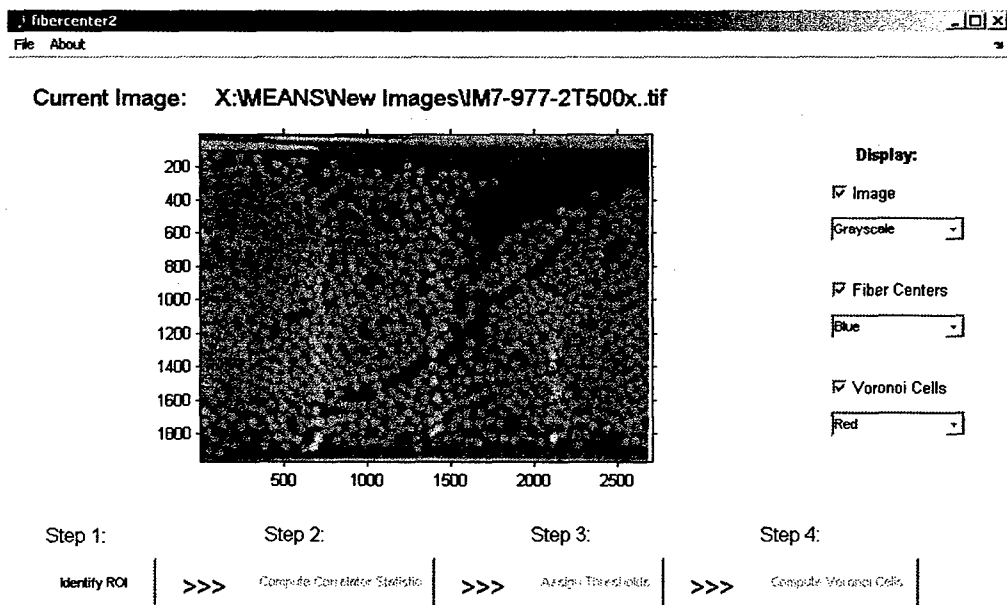


Figure 36 Imported image in the fibercenter program

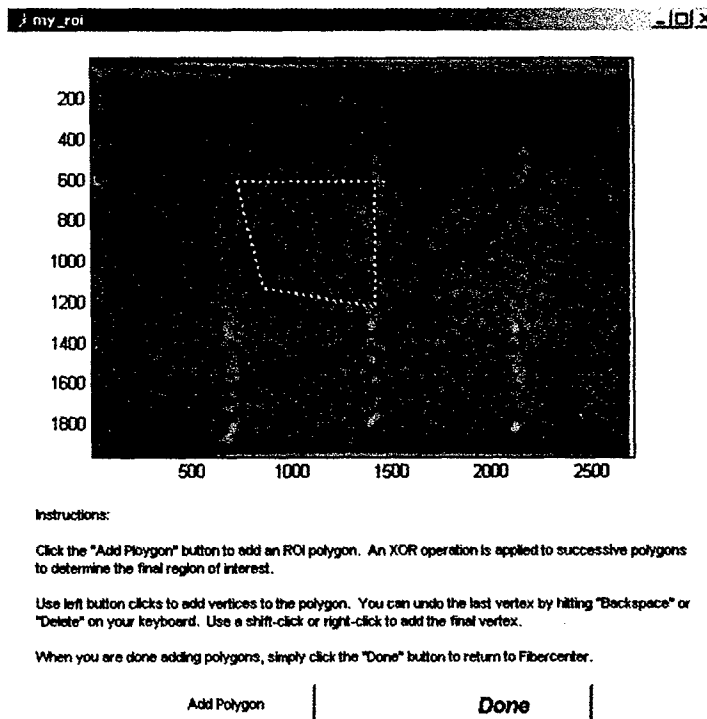


Figure 37 Illustration of Polygon feature used to identify a region of interest (ROI) in image

A polygon feature is activated when the 'Identify ROI' step is selected, as shown in Figure 37. The entire image may be selected for analysis or a subsection may be identified using the polygon feature. When Step 2 (Compute Correlator Statistic) is

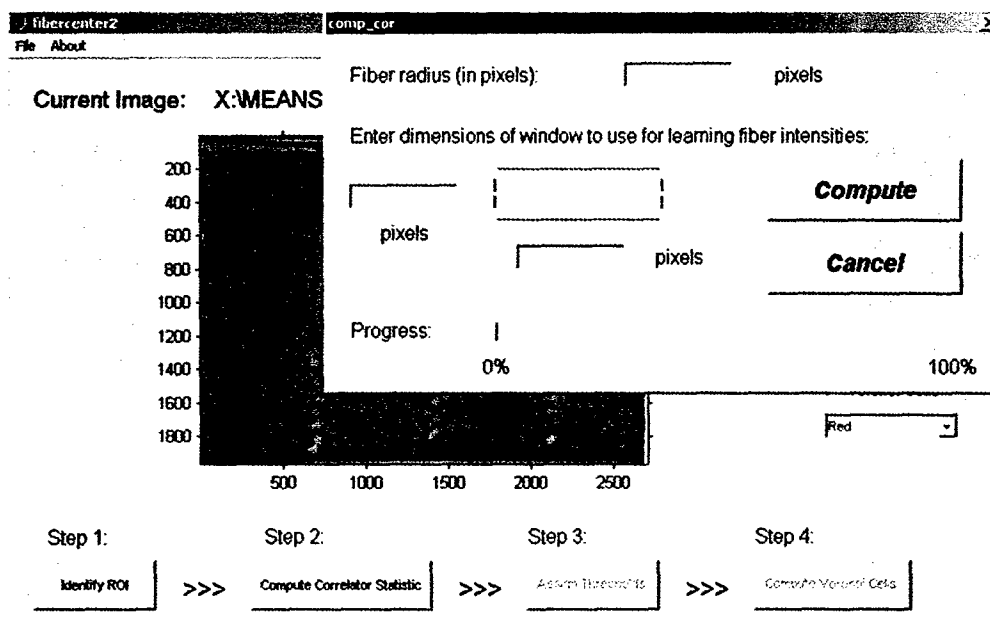


Figure 38 Correlator statistic dialog box

activated another dialog box appears as shown in Figure 38. This asks for the fiber radius in pixels as well as the dimensions of a window (also in pixels) that is used to 'train' the program to identify fibers within the image. The dimensions of the entire image could be chosen, though experience has shown that a window measuring approximately six by six fiber diameters allows the training process to be completed in a reasonable timescale and yields accurate fiber center data. Determination of an accurate value for fiber radius is critical to the accuracy of the resultant data however. This is best achieved by opening the image in any commercially available image viewer (e.g. Photoimpact) and using the highest magnification that will allow individual pixels to be viewed at the same time as full fiber ends. The fiber radius can then be determined in terms of pixels by simply counting the number of pixels across a fiber diameter. This should be carefully repeated a number of times to yield a reliable value. Note that while this may be somewhat time consuming, it will not have to be repeated for images captured under the same magnification and with the same fibers. Therefore once the number has been determined for a sample image it can be used for all similar images.

The next stage in the process is to assign thresholds to the analysis and this procedure is initiated by clicking on Step 3. The new dialog box, shown in Figure 39, requests two input numbers; correlator threshold and background threshold and also offers the option of using the procedure called 'image opening', described earlier. The correlator threshold sets a lower limit below which all pixels are turned to black, and therefore ignored in calculation of centroid locations. Figure 27 is three dimensional plot of the correlator

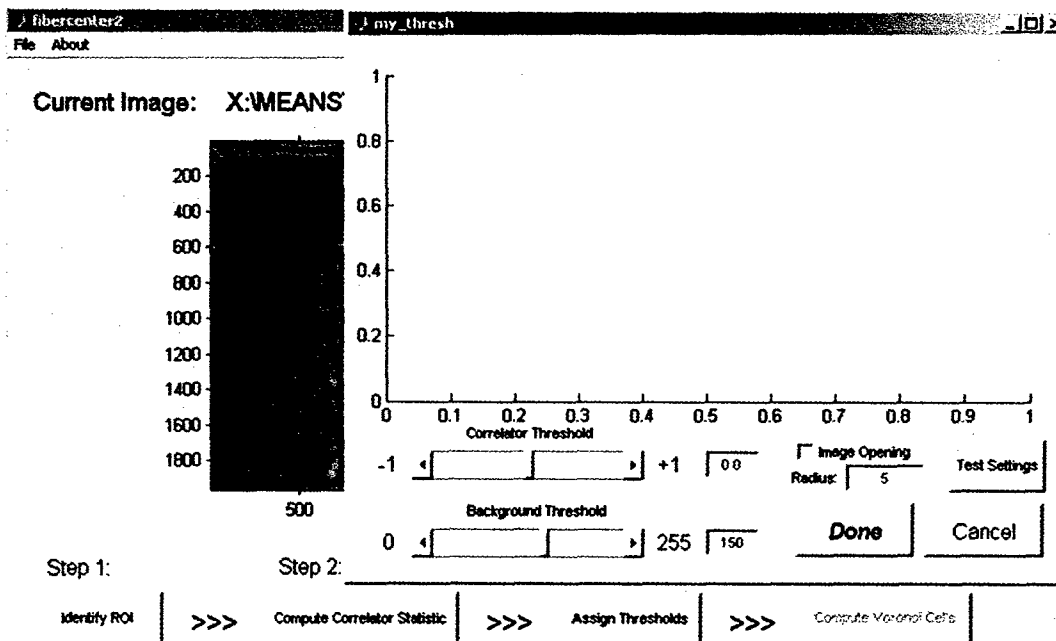


Figure 39 Dialog box used to assign thresholds to a selected image

statistic for the image shown in Figure 26. The objective in selecting this value is to choose a level that eliminates as many 'false positive' lower peaks as possible. The plot of the correlator statistic will then be thresholded at this level to yield the entities that are identified as containing candidate fiber centers. Experience has shown that most images process well with a value between 0.25 and 0.3, so this range should be used to select a starting value.

The background threshold number allows a certain pixel value to be selected as a baseline for the analysis. Essentially this number is subtracted from all pixel numbers before assigning the correlator threshold and has the effect of 'stretching out' the pixel values along the vertical axis in the plot shown in Figure 27. Therefore it allows the thresholding operation to be carried out on pixels that have values above a certain background level. This will vary with the brightness of the image, and some degree of trial and error is necessary to arrive at a suitable number. It should be noted again, however, that when a suitable value is selected for a certain quality image, all similar images will process well with the same value. The program is thus quite tolerant image to image variation. The numbers in this dialog box will generally only need to be adjusted when there is a substantial change in image quality. The final option in this dialog box pertains to image opening. This is a procedure by which entities in the threshold map below a certain size are eliminated from the image. This may be useful in situations where there are features that have similar pixel value compositions as fibers, for example hard grit inclusions, but are distinctly smaller. Note that larger entities are generally ignored if the fiber radius parameter is properly selected. The radius, in pixels, used to perform the image opening process can be input when this option is selected.

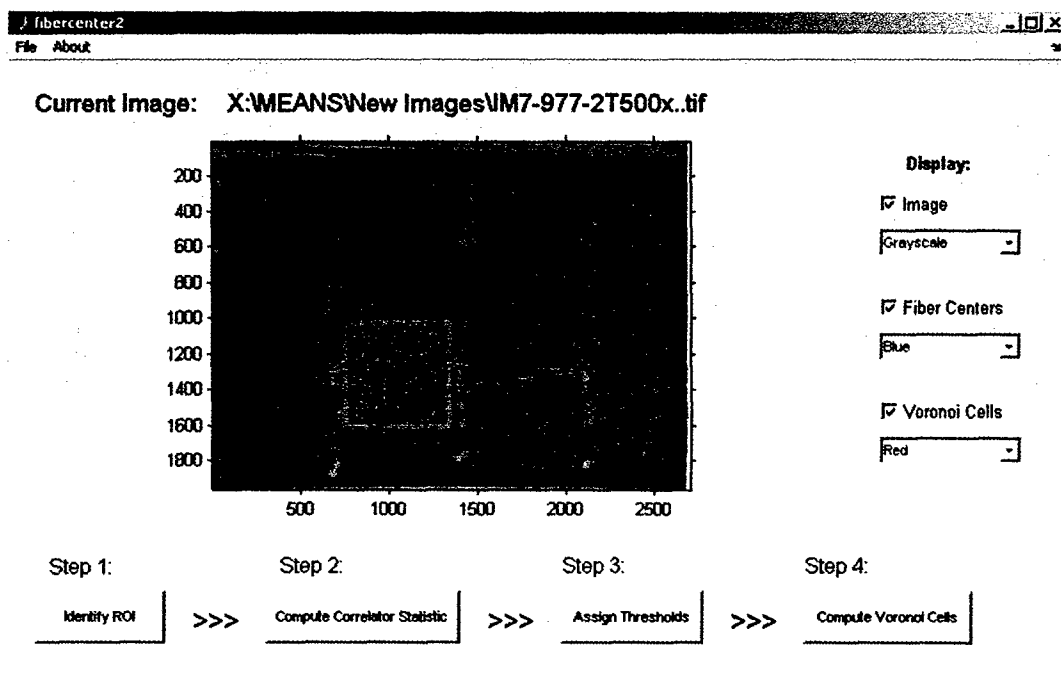


Figure 40 Generation of Voronoi cells in the image Region of Interest

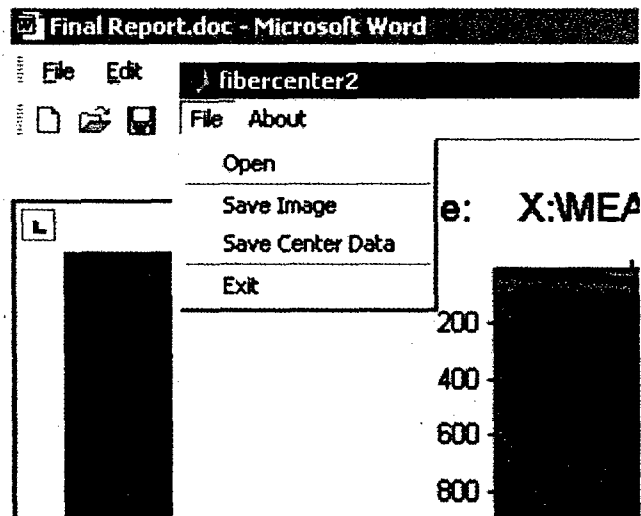


Figure 41 Data saving options in the fibercenter2 program

The final step in the image analysis process is the computation of the Voronoi cells. This is done by simply clicking on the Step 4 virtual button. The result is shown in Figure 40. Notice from the example shown that all fibers outside the region of interest are ignored, and so the Voronoi cells for some of the ROI are not reasonable. This edge effect occurs in all image analysis of this type, but the resultant data can be easily discarded in later data processing.

The fibercenter2 program allows a number of data output options, as shown in Figure 41. The entire image including the Voronoi cells may be saved in Bitmap, TIFF or JPEG formats. The fiber center data may be saved as a tab delimited text file, which can be conveniently imported into spreadsheet or finite element translator files, or as a MATLAB file which is used by the fvplot program to provide fiber volume fraction maps and associated gradient data.

Further manipulation of the image analysis data is achieved by launching the fvplot program from within MATLAB. The initial dialog window is shown in Figure 42, with the 'File' drag down menu activated. The first step in the fiber volume fraction analysis is to open the MATLAB fiber center file (*.mat) generated by the fibercenter2 program. When these data have been imported the fvplot program can be used to plot the corresponding fiber volume fraction data in a number of ways. The IMAGESC – CONTOURF option buttons allow the data to be plotted in raw form or as a fiber volume fraction contour map as desired. The averaging window value is a pixel dimension of a square region that is used to generate the contour plots. The degree of data smoothing that is employed in contour plots will increase with this selected value. The window also allows the number of contours (effectively the fiber volume fraction intervals) to be selected, and the principal selection buttons allow the averaging function to be turned on or off as desired.

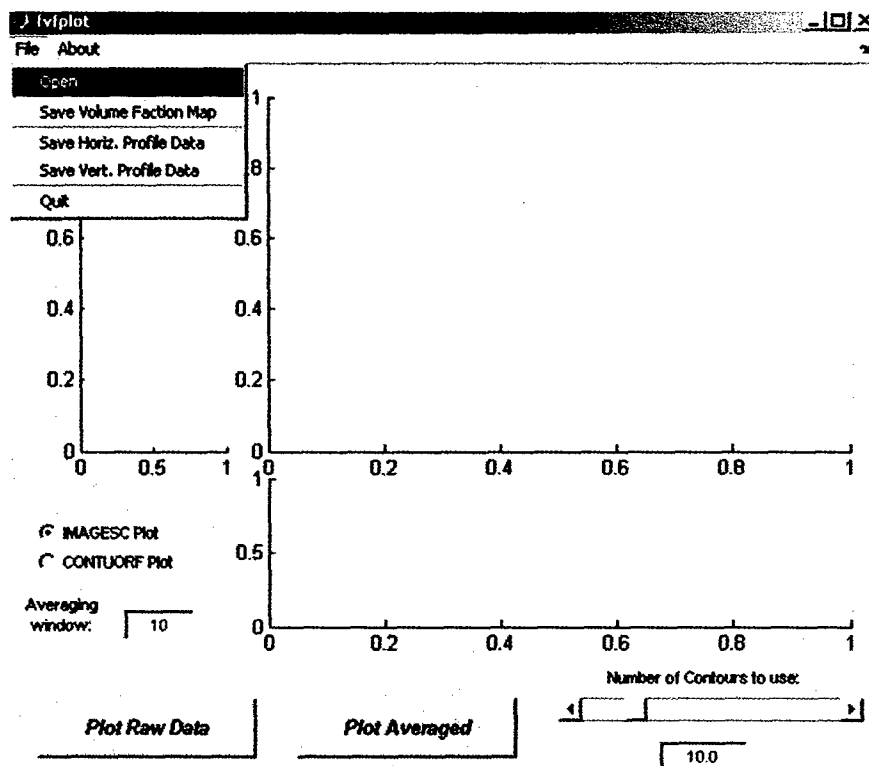


Figure 42 Initial dialog box in the fvplot program

Figure 43 shows an example of the data generated when the Plot Raw Data option is selected. The output is a pixel by pixel representation of the fiber volume fraction based on the Voronoi cell analysis. The program also automatically generates fiber volume fraction gradient plots in the vertical and horizontal axes. This is essentially a raster scanning process. For example, the values plotted for the horizontal axis are generated by averaging the pixel values of fiber volume fraction in the vertical line above the horizontal axis value. The values for the vertical axis are determined in an analogous fashion. All zero values (shown as the dark blue non-analyzed background) are ignored in this calculation. However in this example the values are skewed to lower values by the data from the 'edge' cells that are not realistic representations of the local packing. This problem will be corrected in later versions of the code. However this problem can be eliminated by importing images that are sized to the area of interest. Therefore in such cases the fibercenter2 program is used to analyze the entire image and the ROI polygon feature is not employed.

Similar data saving options are provided in the fvplot program as those available in the fibercenter2 code. As shown in Figure 41, the fiber volume fraction map can be saved in any one of the three previously identified image formats. Also the vertical and horizontal fiber volume fraction profile data may be saved as tab delimited text files or in MATLAB (*.mat) source format for further analysis.

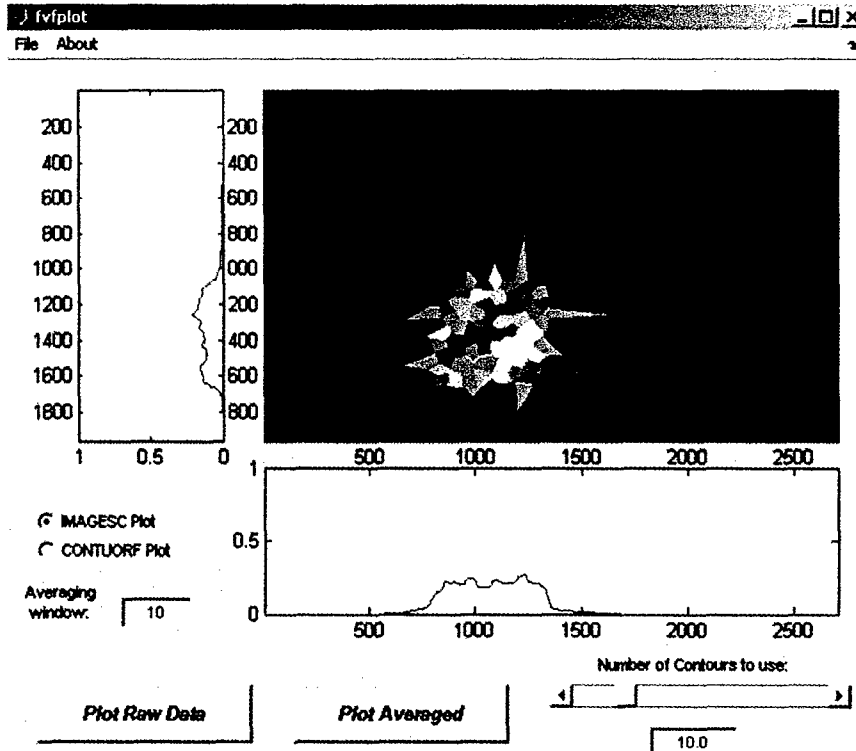


Figure 43 Typical image output from fvplot program.

The automated image analysis tools described above have applicability to a number of analytical problems and approaches. By exercising these capabilities at a number of different length scales it will be, and has already been, possible to generate fiber volume fraction data for real microstructures with unprecedented efficiency. The critical length scales of important architectural features can be identified and large amounts of data can be generated for application of statistical analysis techniques that may be aimed at uncovering salient patterns and data structures as they relate to variations in performance. However the preliminary application of this tool in this program has been directed to occurrence of micro-cracks in transversely loaded composite laminates. The following section details how this initial use of the tools described above has yielded interesting, though not conclusive, insights into the occurrence of such failures.

3.1.2 Application of Automated Image Analysis to Micro-cracking

The automated image analysis software described in the previous sections was applied to a number of examples of micro-cracked composites, both from laminates made and tested in the course of this study and legacy images taken from prior publications. Figure 44 shows a YLA prepreg laminate fabricated by autoclave molding from material produced using the optimal prepregging process. The micrograph shows the central ply of a $(0/90)_{2S}$ laminate that was pulled in tension (along the horizontal axis as shown) until the onset of transverse ply cracking.

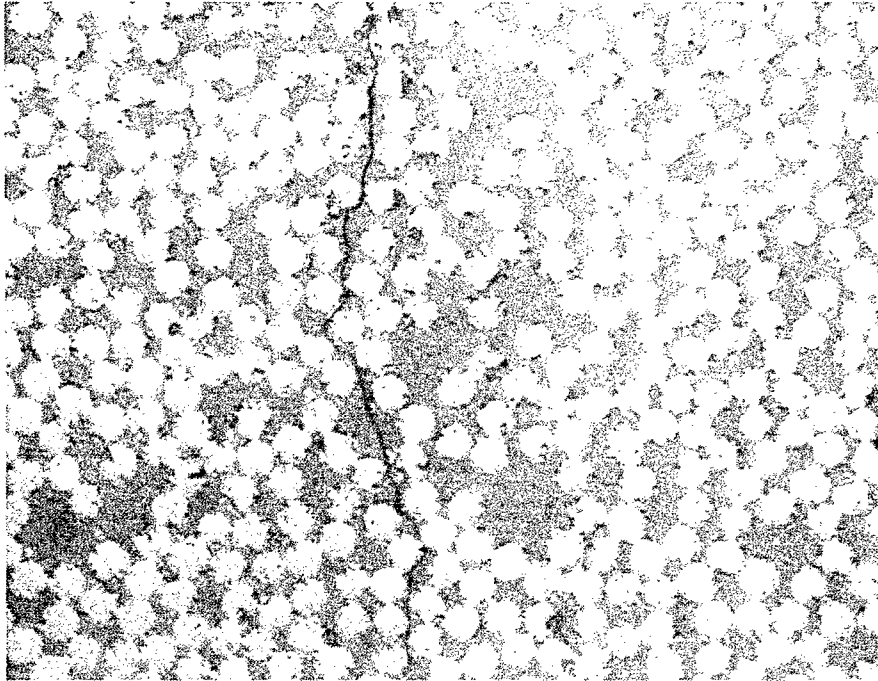


Figure 44 Central ply of a (0/90)2S laminate tested to onset of microcracking

The fiber centers and associated Voronoi cells for this image are shown in Figure 45. Note that the fiber center identification accuracy is in this case 100%, and therefore the resultant fiber volume fraction mapping would also be expected to similarly accurate. Figure 46 shows the mapping for this microstructure with the crack path highlighted in red for clarity.

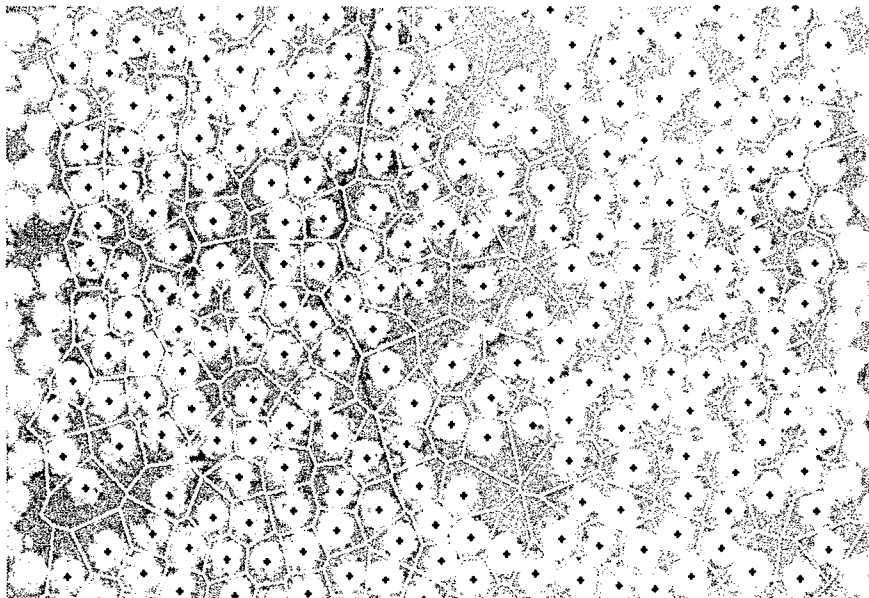


Figure 45 Fiber centers and associated Voronoi cells for laminate shown in Figure 44.

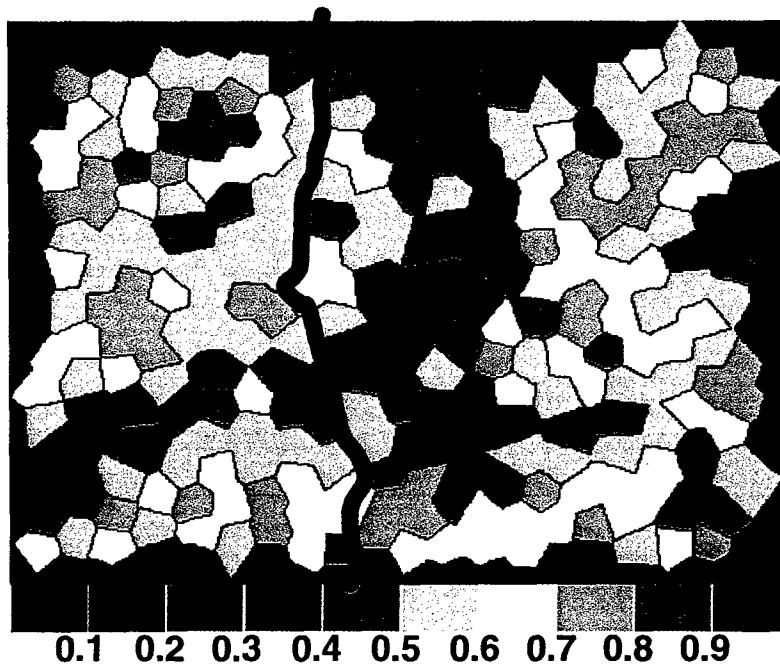


Figure 46 Fiber volume fraction map for micro-cracked composite laminate made from YLA material

Visual inspection of the fiber volume fraction map suggests that the crack path follows the generally low fiber volume fraction regions, but more importantly it seems that it is close to the region in which the fiber volume fraction *gradient* is greatest. Figure 47

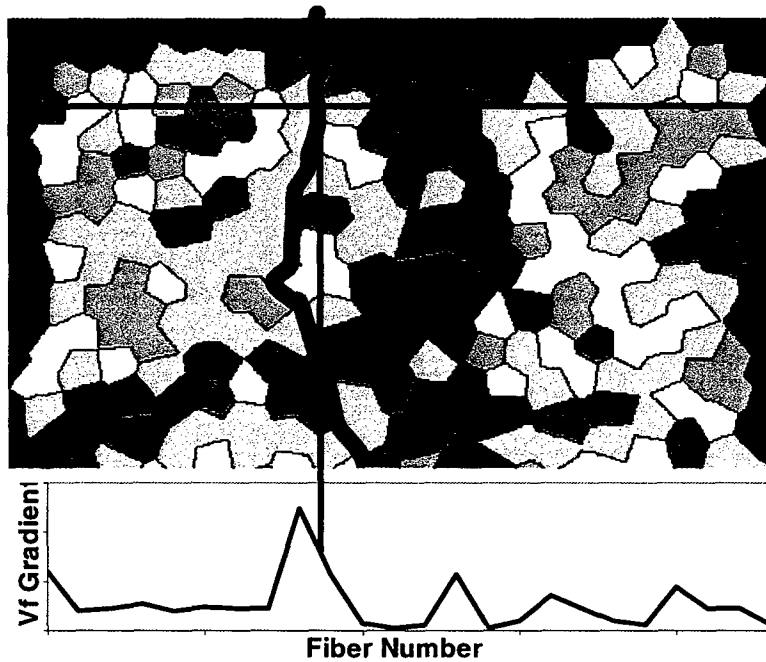


Figure 47 Fiber volume fraction map showing gradient plot across a selected horizontal line

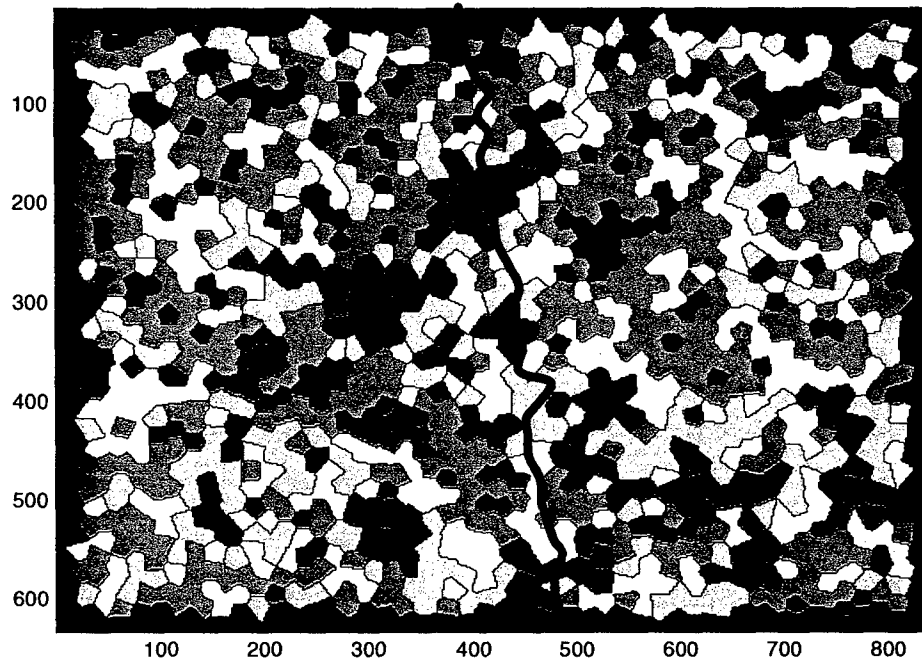


Figure 48 Fiber volume fraction map for large fiber assembly with crack path highlighted

shows the same data presented in Figure 46 but with a plot of fiber volume fraction gradient over the horizontal red line shown for illustration. This is a typical effect seen repeatedly in this study where local crack paths have a tendency to follow regions of high fiber volume fraction gradient. It is important to note that this is simply a preliminary observation, and that significant further study will be necessary before it can be concluded that this is an indicative trend. However, additional micrographs show a similar effect on longer length scales and in larger assemblies of fibers. Figure 48 gives the fiber volume fraction map for such a micrograph. In these examples averaged fiber

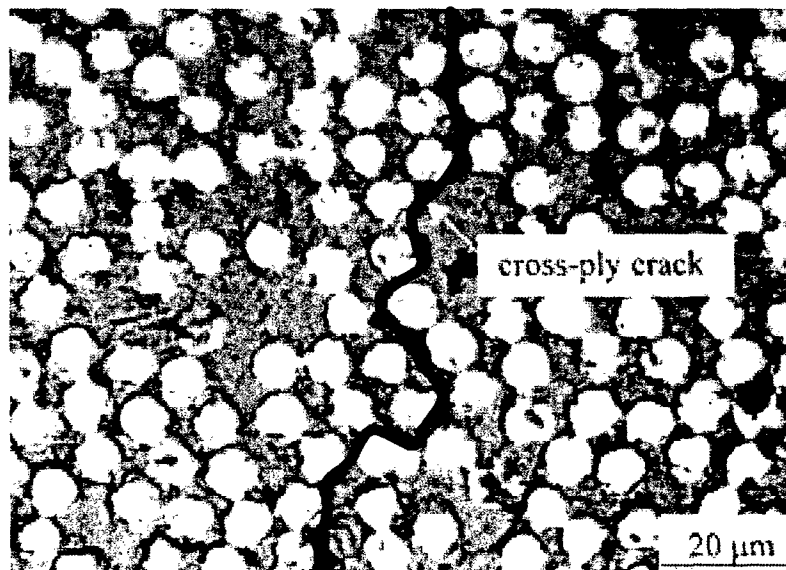


Figure 49 Scanned reproduction of micro-crack image published Abry et.al in 2001

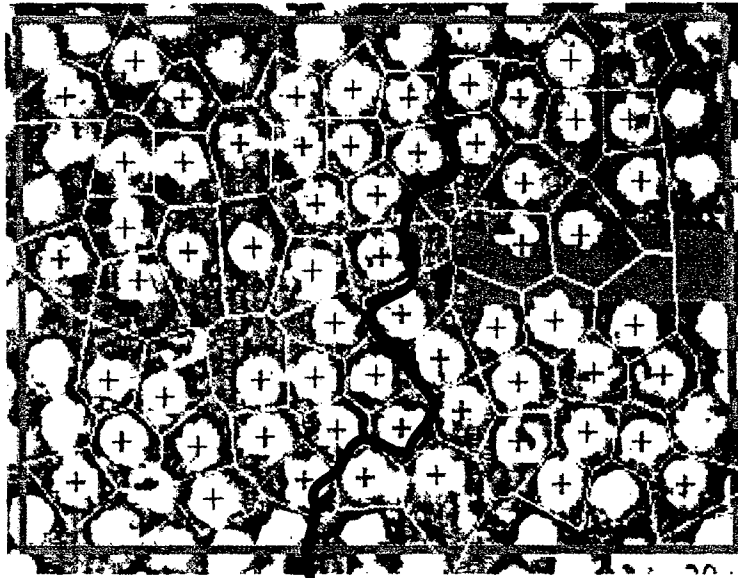


Figure 50 Scanned Voronoi cell analysis of image shown in Figure 49

volume fraction values evaluated in the vertical direction and orthogonal to the load path show a peak in the region of the crack path, though because of the large number of fibers being used to calculate the average the effect is frequently subtle. Whether this observation proves to be significant in terms of micro-cracking mechanisms remains to be seen. However the exercises presented above do illustrate the broad utility of the automated image analysis tool in developing data at varying length scales that may influence performance.

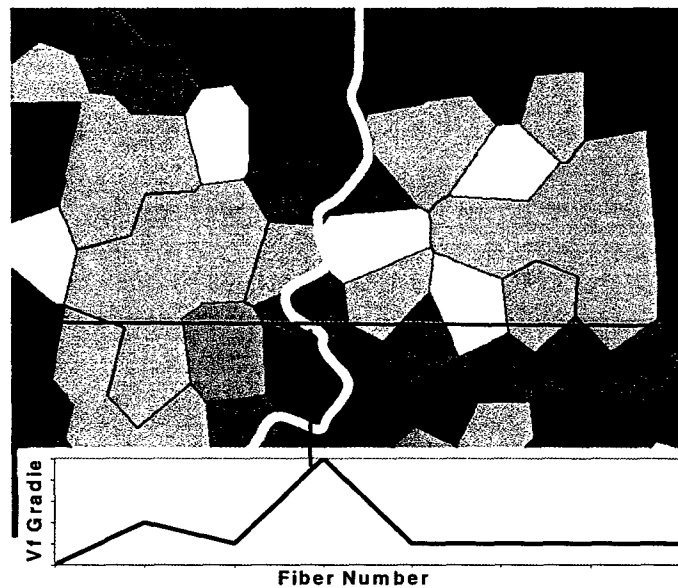


Figure 51 Fiber volume fraction map and associated gradient plot for Abry et. al. image

Similar analyses were performed on previously published micro-crack images. Figure 49 shows an image of a micro-cracked composite laminate that was published by Abry et.al. in 2001 [3]. The crack path has been highlighted as in previous examples. In Figure 50 the annotation on the original image has been removed using the 'paint' function of the Photoimpact program. Almost all commercially available image viewing software packages provide such a facility. The Voronoi cell analysis of the image is also shown in Figure 50. Despite the relatively poor quality of a scanned reproduction of an old journal image the automated analysis was capable of accurately analyzing the image. Figure 51 shows the corresponding fiber volume fraction plot for this image, along with a representation of the gradient along a selected, though representative, direction aligned with the principal loading axis. Though this represents an analysis of a relatively small region the trends suggested by data generated using samples fabricated and tested as part of this program are generally confirmed.

In summary, the automated image analysis tool has provided the capability to conveniently and rapidly characterize the fiber volume fraction distributions and gradients in micrographic images of laminated prepreg composites at a range of length scales. Data export for further analysis can also be achieved with great efficiency. The capability assessment exercises presented here build confidence that length scales ranging from that of the fiber to the laminate can be quickly characterized with attendant facility for statistical data generation that is unprecedented.

3.2 Prepreg Microscopy

Significant program effort was devoted to the development of a means of studying unprocessed prepreg microstructures. When raw prepreg material was mounted in Phenolic resin, in the conventional metallographic manner, unacceptable smearing and fiber pullout occurred, and no usable images resulted. Mounting the prepreg in room temperature curing (Jet Set) epoxy material led to a similar outcome. Some initial success was achieved by applying a technique that involved mounting the prepreg sample in the Jet Set epoxy and applying 60 psi in a pressure pot while the resin cured. Figure 52 shows the resultant 'panoramic' micrograph and two selected areas of interest. Several areas are evident in the micrographs in which the fiber structure appears relatively clear. However the architecture was frequently obscured by, what are believed to be, regions in which resin has been leached out during the polishing process. Closer examination, as provided in Figure 53, also revealed a third 'phase' of foreign material, which is almost certainly embedded abrasive from the sequential grinding processes. While yielding some useful information on fiber arrangements in unprocessed prepreg material such surfaces are not suitable for automated image analysis. Pressurization of the prepreg material also leads to some consolidation as illustrated in Figure 54. The mounted prepreg material is shown alongside an end view of some un-mounted material, and the corresponding surface profiles, as drawn in an image analysis program, are shown

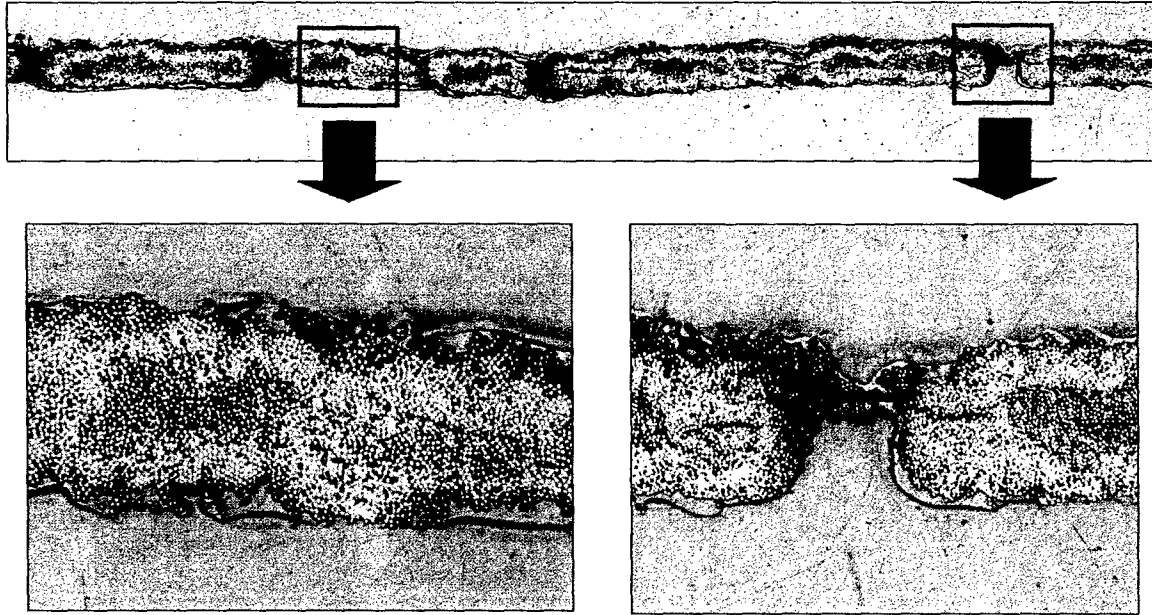


Figure 52 Graphite Fiber Prepreg Mounted in Room Temperature Epoxy under 60 psi Pressure

beneath. The consolidating effect of the pressurized mounting resin is reflected in the reduced thickness relative to the free-standing material.

None of the above results are believed to be satisfactory, at least from an image analysis standpoint. In later program period techniques arising out of biological research were assessed, including cryogenic polishing and microtoming. However these techniques did not provide a viable solution, primarily because of the huge differences in stiffness and strength properties between the resin and fiber phases. The most successful technique developed involved mounting the prepreg material in room temperature epoxy,

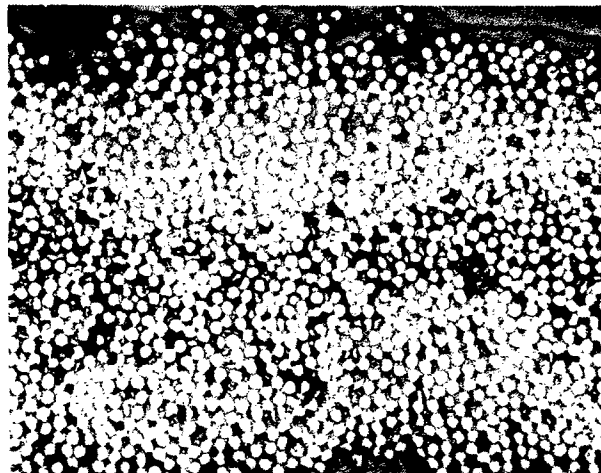


Figure 53 Aligned Graphite Fiber Prepreg Material Mounted in Room Temperature Epoxy under 60 psi Pressure

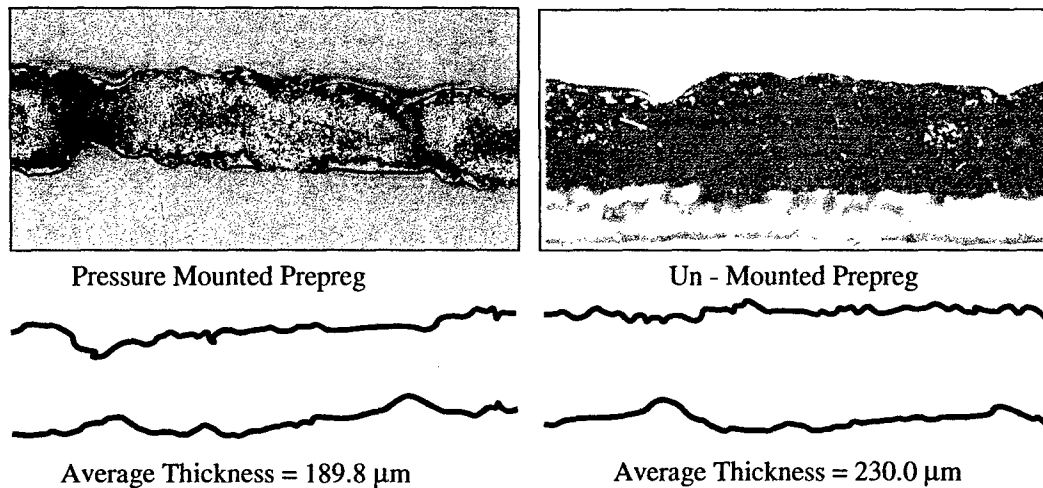


Figure 54 Aligned Graphite Fiber Prepreg Material, Pressure Mounted and Free Standing, with Associated Thickness Profiles

preliminarily polishing the surface and then infiltrating this free edge with a low viscosity rapid cure polymer before re-polishing. This provided the support to the fiber network that is necessary during the polishing process but is not available from the uncured resin.

The two-stage mounting and polishing procedure provided significantly improved results. In this procedure the prepreg material was mounted in a room temperature rapid cure epoxy. No pressure was applied while the resin was being cured. The sample was then subjected to the normal polishing procedure to provide a flat surface for the second stage of the process. The sample was then immersed in the room temperature cure epoxy and vacuum was applied in order to remove as much of the air from the void regions at the polished surface as possible. Pressure of about 60 psi was then applied to the epoxy as it cured. The sample was then subjected to the same polishing procedures as before, but care was taken to remove as little of the existing polished surface as possible. The idea behind the technique is to fill in the vacant spaces in the prepreg cross section with hard resin. This supports the fiber network during polishing so that the fibers are basically held in place by the cured epoxy and b-staged matrix. The resultant quality is evident in Figure 55 (and also in Figures 29 and 31) where image quality is equal to that of fully cured laminates.



Figure 55 Uncured Prepreg Material Mounted and Polished using a Two- Stage Process

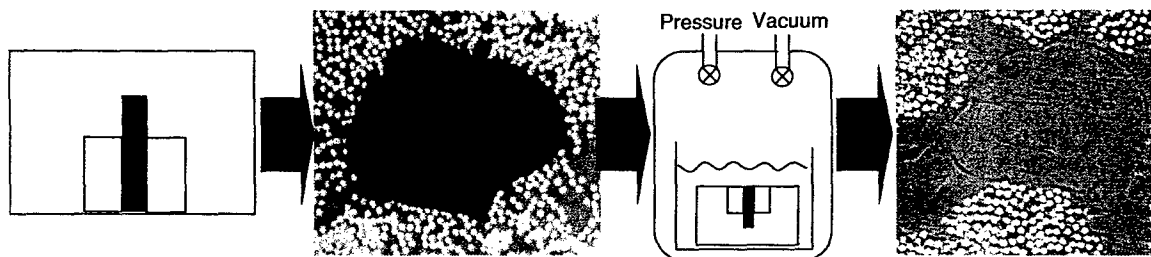


Figure 56 Illustration of two stage mounting process used to produce micrographs from uncured prepreg

The two stage process is illustrated in Figure 56. The procedure begins with the mounting of a strip of prepreg material in a room temperature cure e.poxy system. This sample (shown schematically in the right side of Figure 56) is then polished in the conventional fashion using successive silicon carbide grit papers ranging in grit size from 320 to 1200. The sample is then subjected to a 1 μm or 3 μm diamond paste polish. Figure 56 shows a large void in the prepreg material that is typically evident after this polishing phase. The unsupported material around this hole allows the type of material movement to occur during grinding and polishing operations that leads to the relatively low quality images shown previously. The idea behind the second stage of the mounting procedure is to infiltrate such regions with material that will harden in place and then support the surrounding uncured prepreg in the second polishing stage. The infiltration stage is essentially a resin transfer process. The polished sample (still mounted in epoxy) is submerged face up in a container of uncured epoxy. A range of different epoxies are suitable for this application with the principal requirements being low mix viscosity (on the order of 200 cP or less) and short cure time (preferably less than 15 minutes). The submerged sample is then placed in a pressure pot, as shown in the right middle image in Figure 56, and vacuum is drawn to remove air from the holes in the prepreg architecture. Vacuum is held for about 5 minutes after which the vacuum valve is closed and pressurized air is admitted to the pressure pot. A pressure of 60 psi was used in this study, though higher pressures could also be employed. The resultant sample is then carefully ground and polished as before. The rightmost image in Figure 56 shows the effectiveness of the procedure. A clear boundary between cured epoxy and uncured prepreg material is seen at the center of the part and it is very apparent that this region contained a hole after the first polishing stage.

It is important to note that the second grinding and polishing stage must remove a substantial amount of material in order to assure that the microstructure revealed is representative of the architecture beneath and not retaining remnants of disturbances caused by the first stage of the process. For this reason it is recommended that between 1 and 3 mm of material be removed in automated grinding and polishing steps, using grits that are no coarser than 1200, but preferably 2400. This may take a long time to complete, but is crucial to assuring that representative microstructures are analyzed. Use of finer grit polishing agents ensures that forces are low and therefore minimizes the risk of fiber movement during the second stage of the procedure.

3.3 Finite Element Analysis

An important area of program effort was in numerical analysis of fiber networks. The initial goal was to develop a finite element model representing the microstructures that were studied in the experimental program, and to gain insight into the effects that microstructure variations have on stress and strain profiles within fiber networks.

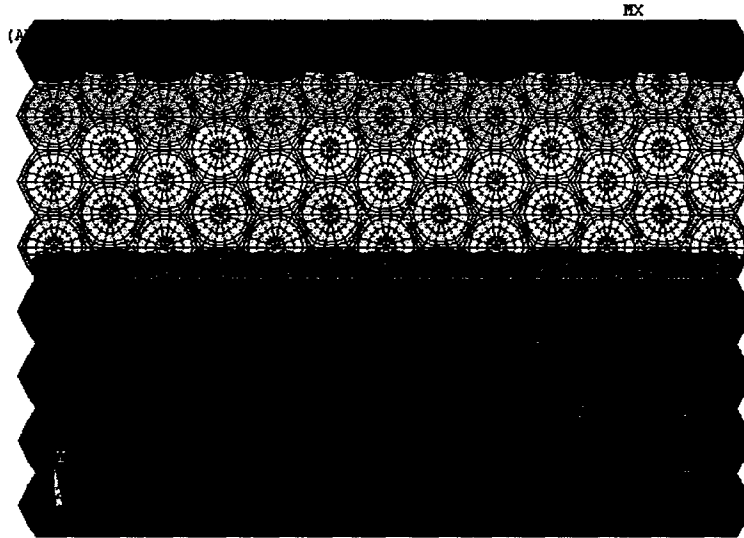


Figure 57 Deformation Contour of the Finite Element Grid Used to Represent a Generic Composite Microstructure

Figure 57 shows the deformation contour of a generic finite element grid used to represent composite microstructures. A regular hexagonal array was used to model the structure. The deformation contour was generated with a rigid constraint boundary condition at the base of the fiber array and a 2% enforced displacement applied at the top free surface. The contour plot shows the increasing deformation levels as the free surface is approached from the 'clamped' base. Typical properties for graphite fibers and epoxy resins were used in the material model.

The internal stress and strain profiles for this structure at three different fiber volume fractions are shown in Figure 58. These fiber volume fractions were chosen to be representative of those observed in three Areas of Interest (AOI) within the laminate used in the early stages of development of the Voronoi cell analysis technique. The figure shows clearly the effects of strain magnification that result from the reinforcement of a typical epoxy with different fiber volume fractions. The stress plots show how the fibers preferentially pick up load and this load is locally passed into the lower stiffness matrix with a resultant increase in strain. This effect becomes more pronounced as the fiber volume fraction is increased, with the result that, even at relatively low laminate strains, matrix strains could reach failure levels. This effect emphasizes the fact that fiber architecture variability will, likely, have a greater effect on laminate strength and durability parameters than on stiffness.

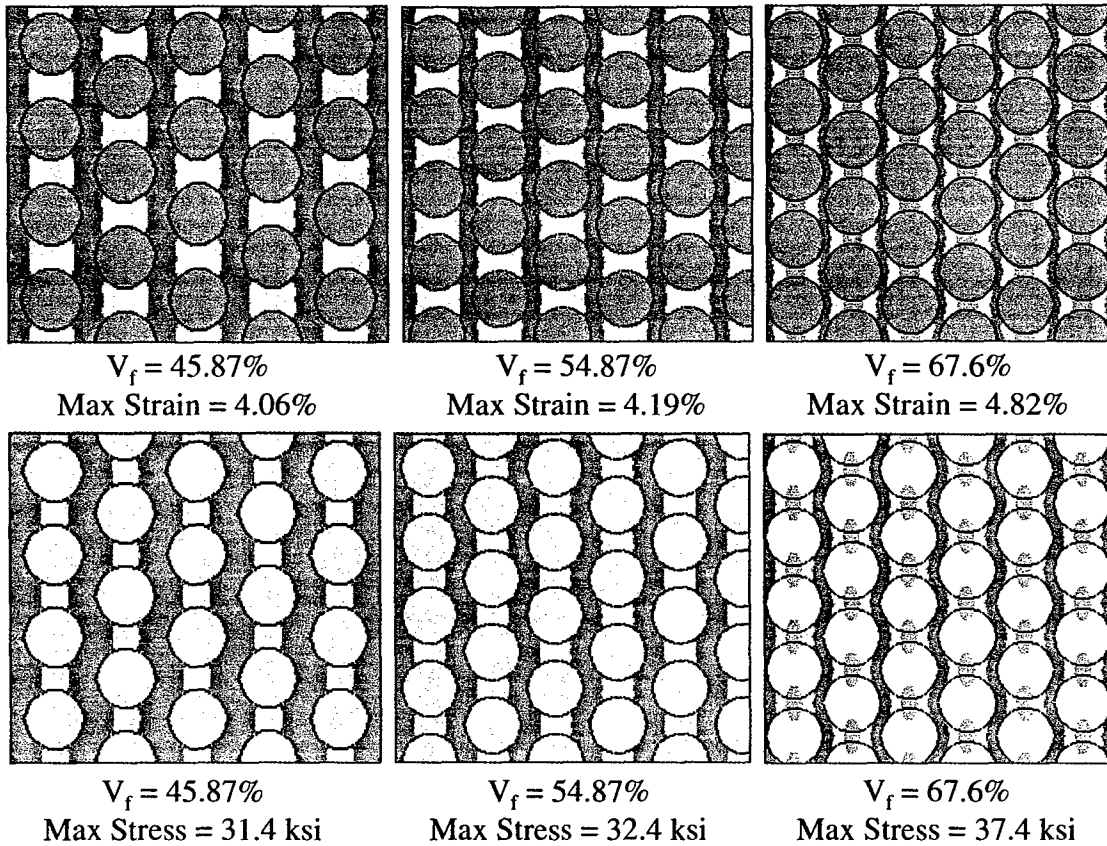


Figure 58 Internal Strain and Stress Contours for Regular Hexagonal Fiber Arrangements at Three Different Volume Fractions

In order to begin to capture some of these variability effects, fiber scale variations observed in the micrographic analysis were duplicated in the finite element model. This was achieved by assigning matrix properties to the fiber elements in a pattern representative of 'real space' observations. The resultant model is shown in Figure 59,

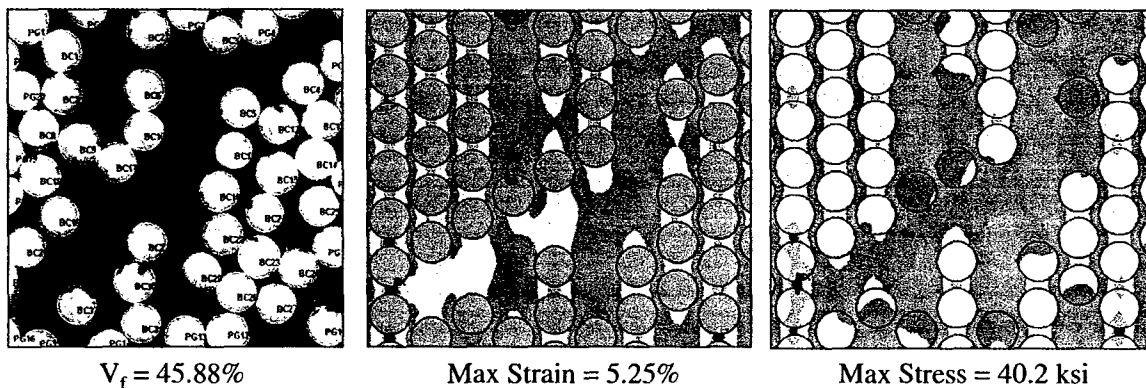


Figure 59 Micrograph of Intermediate Level Fiber Packing Region and Associated Internal Strain and Stress Finite Element Models

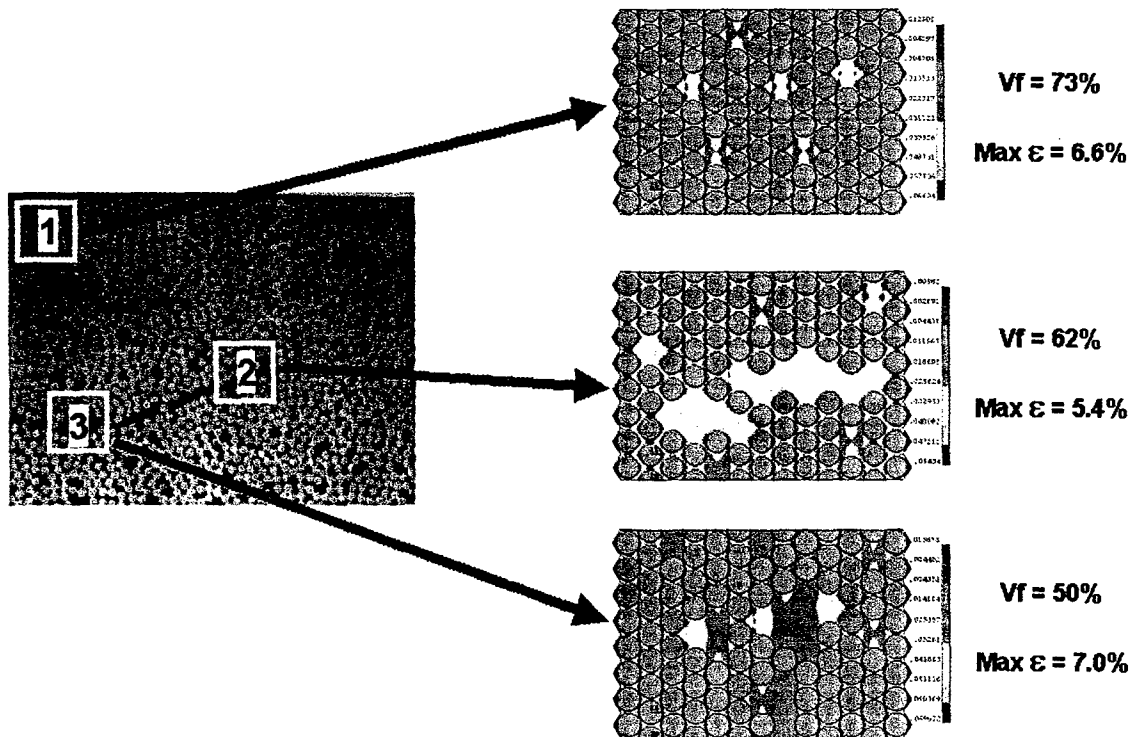


Figure 60 Internal Strain Contours for Observed Fiber Arrangements in Areas of Interest (AOI's) 1, 2 and 3 of Carbon/Epoxy Laminate

again with a 2% enforced displacement, alongside an actual microstructure. Note that the model does not precisely represent the microstructure presented, since fibers that were not removed are arranged in a regular hexagonal array. This problem was eliminated in later work when an automatic mesh generated scheme, based on the Dirichlet tessellation method, was applied. However the data do show the principal fiber scale impacts of material variation. It is apparent from the stress and strain contours that the 'irregularity' of the fiber packing leads to the formation of regions in which stress and strain levels are greater than those seen in the regular array. In the regularly packed 45.88% fiber volume array the calculated maximum strain was 4.06% with an associated stress of 31.4 ksi. The corresponding levels in an irregular array with the same fiber volume fraction are almost 30% higher. This shows the enormous impact that material variability can have on mechanical performance, particularly strength and durability parameters.

In order to shed further light on variability effects, some of additional fiber scale variations observed in real laminates duplicated in finite element models. Several micrographs from the central plies of the YLA laminate were examined and Areas of Interest (AOI's) were selected that were thought to represent the practical variation in fiber arrangements throughout the composite panel. Again the results of FEA determination of strain patterns caused by application of a 2% through thickness deformation are shown in Figures 60 through 62. It should be noted that the FEA microstructures were again generated by omitting selected fibers from an ideal hexagonal grid and then adjusting the fiber spacing to match, as closely as possible, the fiber volume

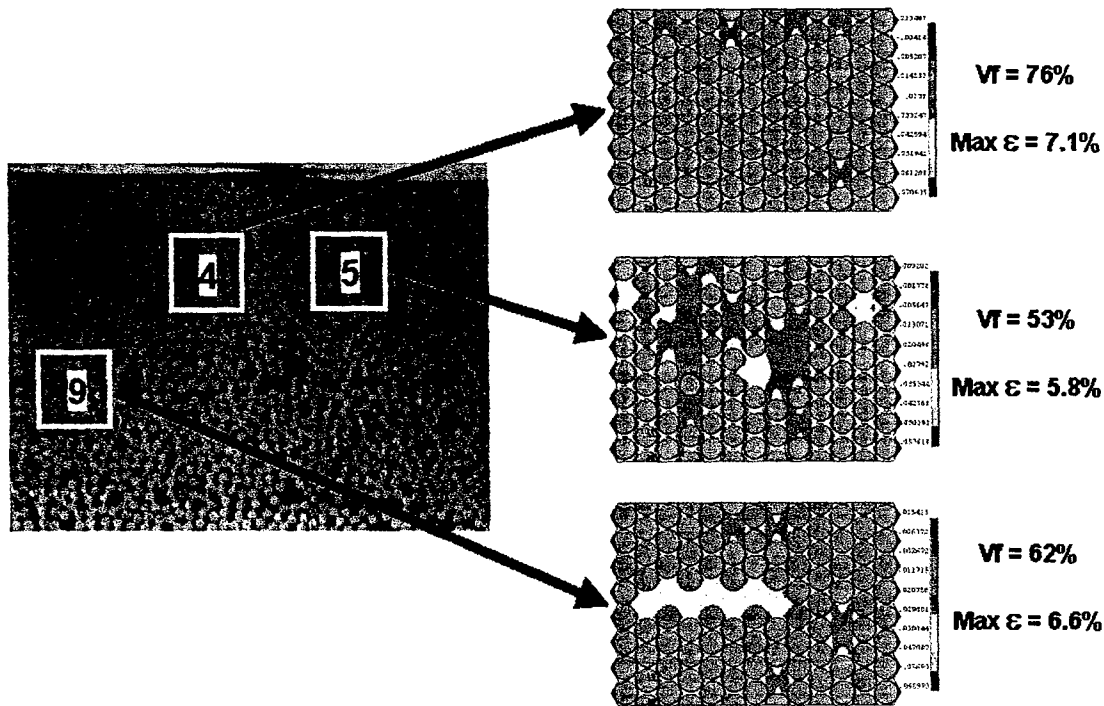


Figure 61 Internal Strain Contours for Observed Fiber Arrangements in Areas of Interest (AOI's) 4, 5 and 9 of Carbon/Epoxy Laminate

fraction measured in the real material using a threshold analysis. As already pointed out, this is a less than ideal method of representing actual microstructures, it does allow the essential effects of architectural variation to be approximated.

The strain magnification effect, previously mentioned, is evident in this series of simulations. The high fiber volume fraction area identified in Figure 60 (73%) shows a relatively broad distribution of high matrix strain regions. By comparison with the intermediate packing region (62%) the matrix strains are generally higher. This is due to the fact that a large compliant region runs horizontally across the microstructure and the strain magnification is relieved by the presence of this low stiffness feature. In the low packing (50%) region very high strain regions are seen. These occur because essentially straight columns of fibers pick up the through thickness load and the low stiffness regions on either side further magnify the strain. Similar effects are seen in Figure 61 except that in this case the maximum matrix strain occurs in the high fiber packing region (76%.) This is because the missing fibers are roughly horizontally aligned and lie along a line only one fiber diameter in thickness. The 'column' effect described above is therefore locally magnified by the presence of a very stiff network. In Figure 62 fiber arrangements taken from more widely spaced regions are shown. The low packing area (48%) represents the worst arrangement from a strain magnification standpoint. Here a low density packing region is almost fully surrounded by material in which the fibers are very close together. At the right hand edge of the resin rich area there are a few fibers that constitute a 'column' and the result is that the matrix strains are locally very high.

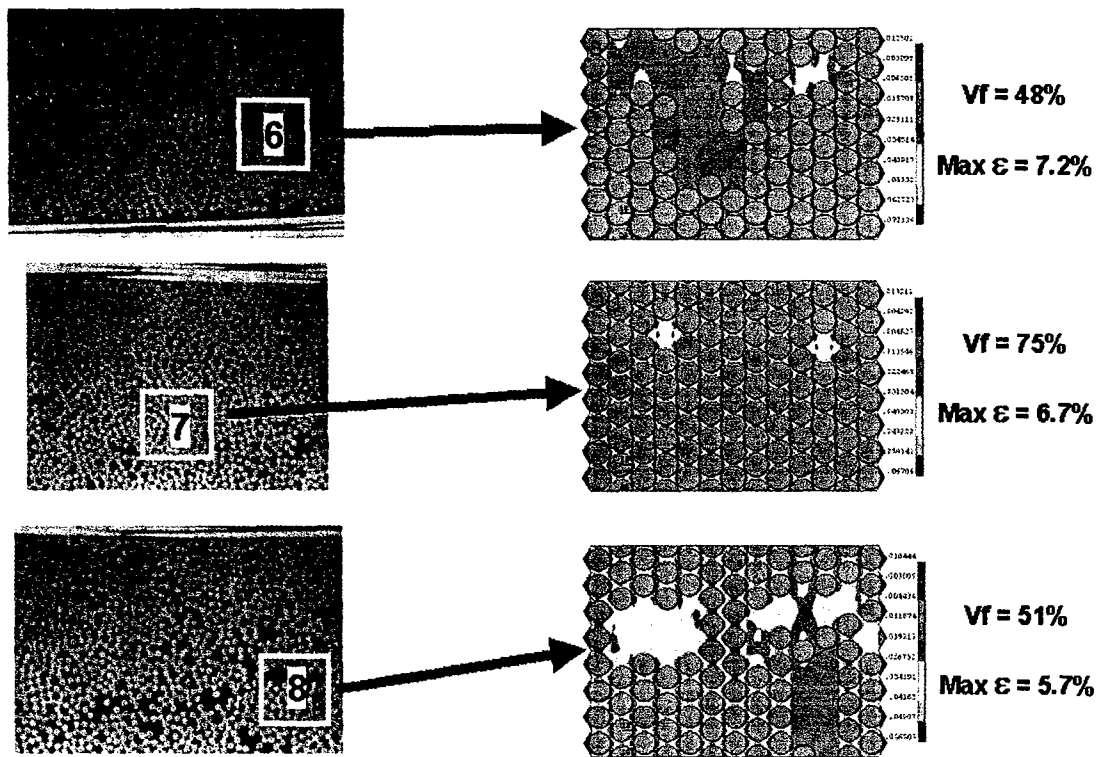


Figure 62 Internal Strain Contours for Observed Fiber Arrangements in Areas of Interest (AOI's) 6, 7 and 8 of Carbon/Epoxy Laminate

The above argument again emphasizes the potentially great impact that fiber arrangements can have on structural response. Of course, through thickness boundary deformations on the order of 2% are not very realistic from the practical applications perspective. Also, more complex in-plane deformations are of greater interest to the design community, but the stress environment considered is arguably the most sensitive to fiber packing variation, and therefore the most likely to assist in the identification of the appropriate length scale for the analysis. Later, program effort was devoted to determining the suitable dimensions of the representative volume element as well as the realistic variations in fiber packing that can be expected to occur within such RVE's. Ultimately this will allow model microstructures to be developed based on realistic variations in packing arrangements, and not some assumed (and probably erroneous) randomization algorithm.

An indication of how the automated image analysis tool might be used to complement FEA of composite microstructures under load was gained in a further analysis of microcracking images from published literature. Figure 63 shows an image published by Lafarie - Frenot et. al.[4] along with the associated Voronoi cell grid. The crack path is highlighted as before. Note that some errors did occur in the image analysis, primarily due to the somewhat irregular cross sections of the reinforcing fibers and the fact that the original image was of relatively poor quality.

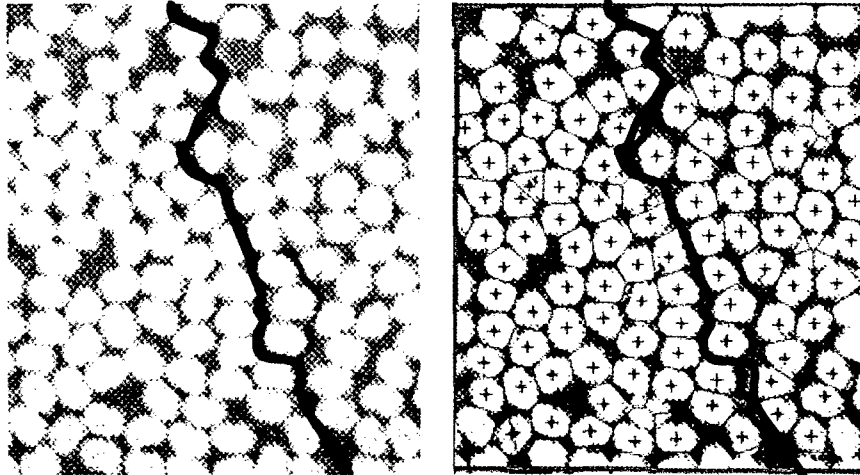


Figure 63 Image of microcracked composite published by Lafarie -Frenot et.al. along with the associated Vornoi cell grid

Figure 64 shows an approximated finite element grid subjected to loading in the horizontal direction, which was the manner in which the actual sample was stressed. The figure also shows the corresponding fiber volume fraction map with a representative gradient plot along a stress aligned path highlighted as in prior examples. The locations of highest strain are circled in the FEA image. The crack path is seen to generally follow the highest strain path which seems to roughly correspond to the line of maximum fiber volume fraction gradient. Again, this is based on very preliminary analysis and significant further modeling will be necessary before any formal conclusions can be made. However the greater significance of the analysis is that it shows how the practical tools developed in this program can be integrated to provide potentially powerful insights into deformation and failure mechanisms that affect the performance of advanced composites.

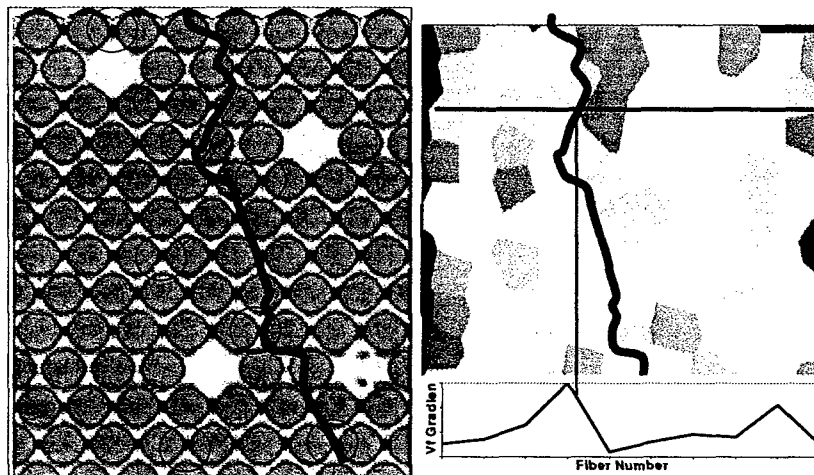


Figure 64 Strain profile developed by horizontal axis stressing of the microstructure published by Lafarie - Frenot et. al. along with the corresponding fiber volume fraction map and selected gradient

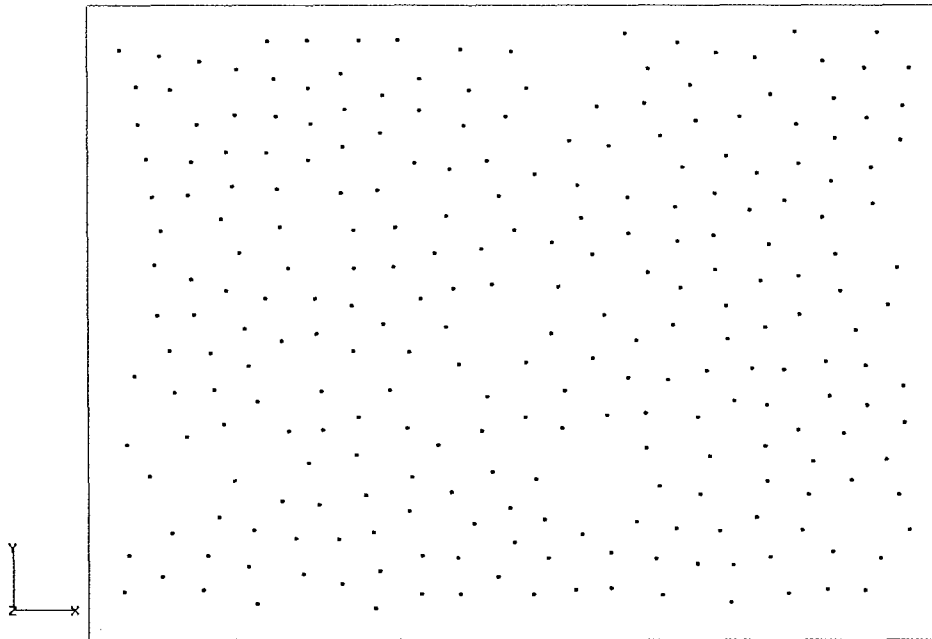


Figure 65 Fiber Centers as Transferred to FEA Mesh Generator

The principal drawback of the analysis presented in previous sections is that it is based on the omission of fibers from an orthogonal array, and the approximation technique thus constituted depends on the judgment of the analyst. A much more realistic grid generation technique would be based on the Dirichlet tessellation method used to characterize variations in fiber arrangements. Therefore finite element analyses based on this approach have been completed to investigate the strength of a composite laminate with irregular fiber distribution. As mentioned above, previous analyses were completed for FEA simulation of regular composite fiber topography with specific fibers removed from the structure.

Analyses were completed at the fiber diameter scale to investigate fiber positioning contribution to structural performance. This latest effort was focused on extension of the previous analysis technique coupled with development of FEA models of actual measured fiber distributions from as-fabricated laminate specimens. Previous sections of this report describe the automated image analysis software that was developed to utilize Voronoi tessellation to generate a FEA mesh of the measured fiber locations in a 2-D plane strain laminate cross-section. The developed FEA models are used to predict the stress / strain distribution through the composite for varying fiber distributions and load conditions.

Micrograph data was acquired for as-fabricated laminate samples which have been tested to micro-crack initiation. The microstructure used to initiate development of this capability is shown in Figure 44. The center point of each fiber is calculated using topographical imaging of the fiber micrograph, and a baseline Voronoi cell set for the test data is generated to estimate fiber volume fraction. Figure 45 shows the calculated fiber centers and Voronoi cells for the micrograph shown in Figure 44.

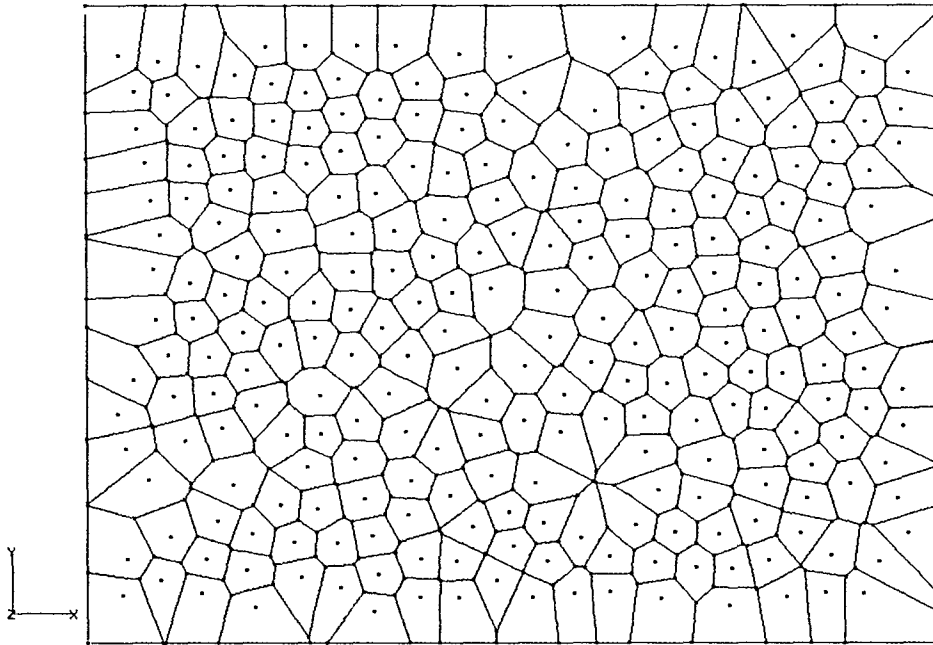


Figure 66 Voronoi Cell Tessellation as Calculated by FEA Mesh Generator

The FEA models are generated by reconstructing the Voronoi cells for the measured data, and subsequently developing a fiber mesh and matrix mesh within each cell. The Voronoi cells are recalculated for the FEA mesh generation rather than using the test data calculated cells directly, since the Voronoi boundary edges must be generated specifically for the FEA mesh. The minimum distance between a fiber diameter and the model boundary edge is a mesh generation variable.

The Voronoi tessellation is constructed by connecting the perpendicular bisector of line segments which connect adjacent points. The Voronoi tessellation has the following characteristic properties, which follow from the definition of the Voronoi cells:

- every Voronoi cell has at least three vertices
- the vertices of a Voronoi cell form a convex hull around the center
- every vertex of a Voronoi cell lies midway between the two centers of the adjacent Voronoi cells
- all points within the area bounded by a Voronoi cell are closer to the Voronoi cell center point than any other point in adjacent Voronoi cells

Figure 65 shows typical fiber center points which are transferred from the measured data to the FEA mesh generator.

Figure 66 shows the FEA model Voronoi cell configuration which is generated by the automated mesher. The interior region of the cell definition is identical to the test data of Figure 45, while the boundary edges have been defined by the model generator to develop a total FEA mesh.

The FEA elements are developed by defining a fiber mesh at each fiber center and filling the remainder of the Voronoi cell with matrix material (see Figure 67). The fiber diameter is a program variable. The FEA mesh is developed using quadrilateral plane

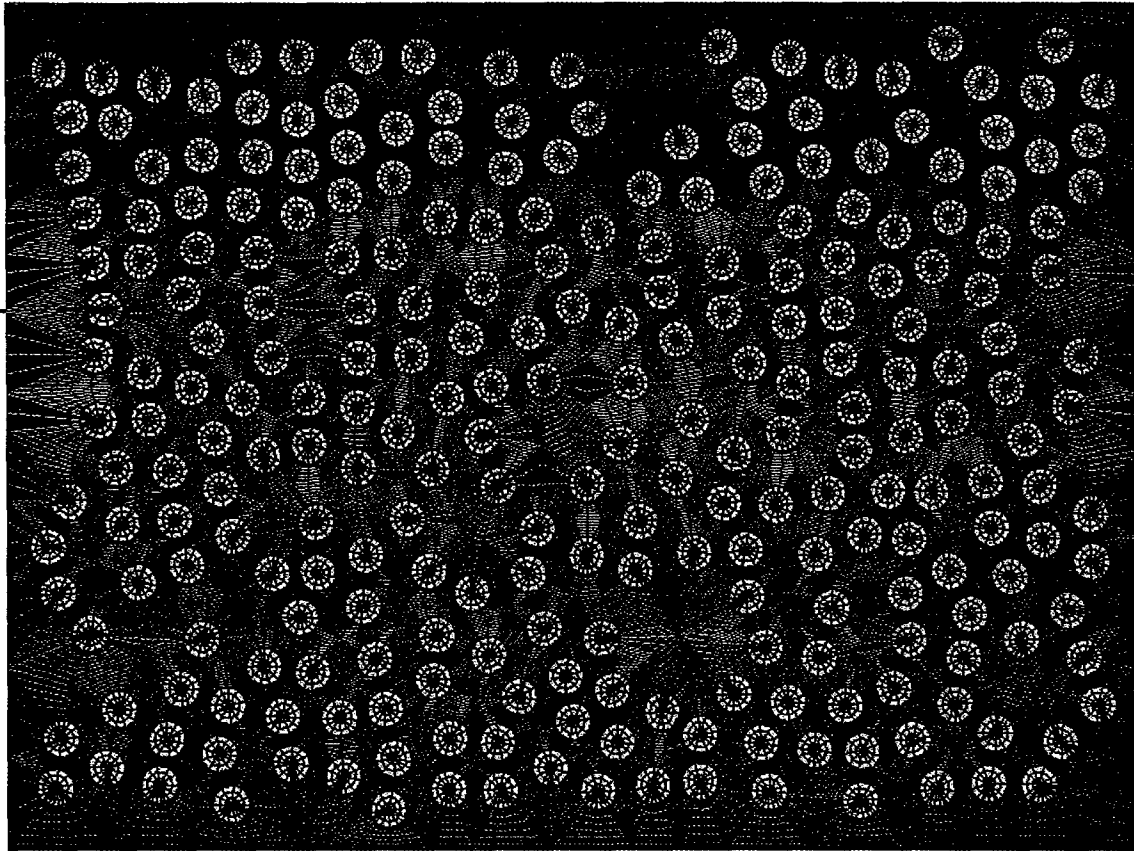


Figure 67 Sample FEA Mesh, as Generated by Automated FEA Mesher

strain elements. The mesh generation logic can be simplified if triangular elements are used for the automated mesh generation, but the quadrilateral elements are superior to triangular elements for stress and strain predictions. The only triangular elements in the automatically generated FEA mesh are at the extreme fiber centers. Mesh density can be varied in the radial and tangential directions for each fiber and Voronoi cell. Additionally, the mesh generation program logic makes additional meshing decisions based on minimum element sizes, acceptable element shapes, and mesh gradients between neighboring cells.

At time of final reporting analyses have been initiated with the developed models to predict sample failures and correlate to measured data, and these efforts will continue into the MEANS II follow on effort. Figure 68 shows a typical FEA result for strain predictions with a uniform edge load applied to the sample. Figure 69 shows typical results for stress predictions for the same mesh. The stress and strain contours are shown to vary with relative fiber position, with higher local strains in regions where the random position of the fibers is preferentially aligned with the load direction. Additional evaluation of these types of stress results will be completed when model correlation data becomes available in the next early phases of the follow on effort.

In addition to the strength based results of Figure 68 and Figure 69 fracture analyses have been completed with the FEA models to predict crack growth across the laminate. Preliminary results have shown numerically biased results which predict crack growth

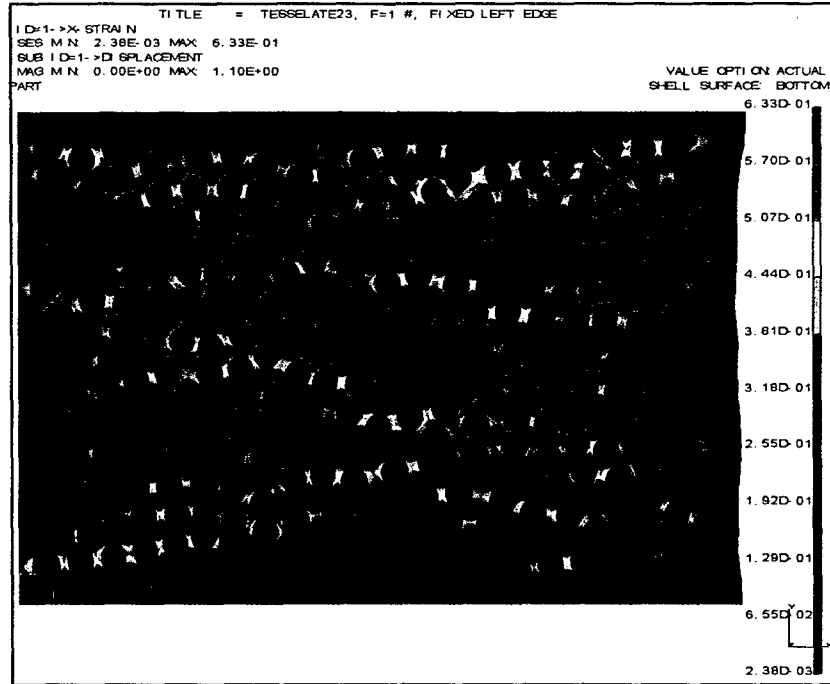


Figure 68 FEA Model, Predicted Strain, Uniform Edge Load at Right Side of Specimen

along the largest element sides. Additional optimization of the automated meshing routines is planned to better configure the meshes for crack propagation analyses.

In addition to the stress and strain data, displacement data for fiber centers can be used for model correlation. Figure 70 shows a typical model result for a displacement contour with a uniform load applied to the sample end. Analysis of test data using the developed

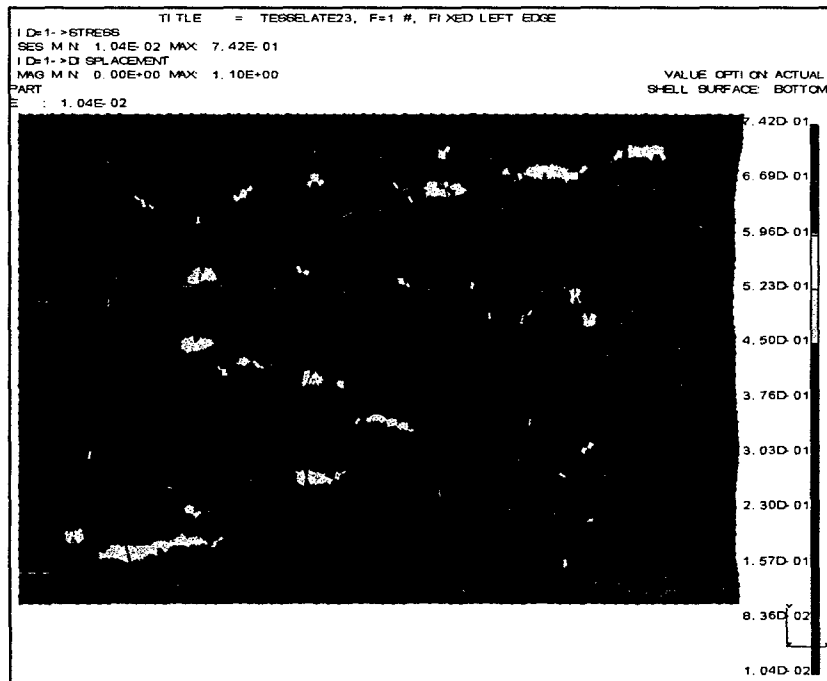


Figure 69 FEA Model, Predicted Stress, Uniform Edge Load at Right Side of Specimen

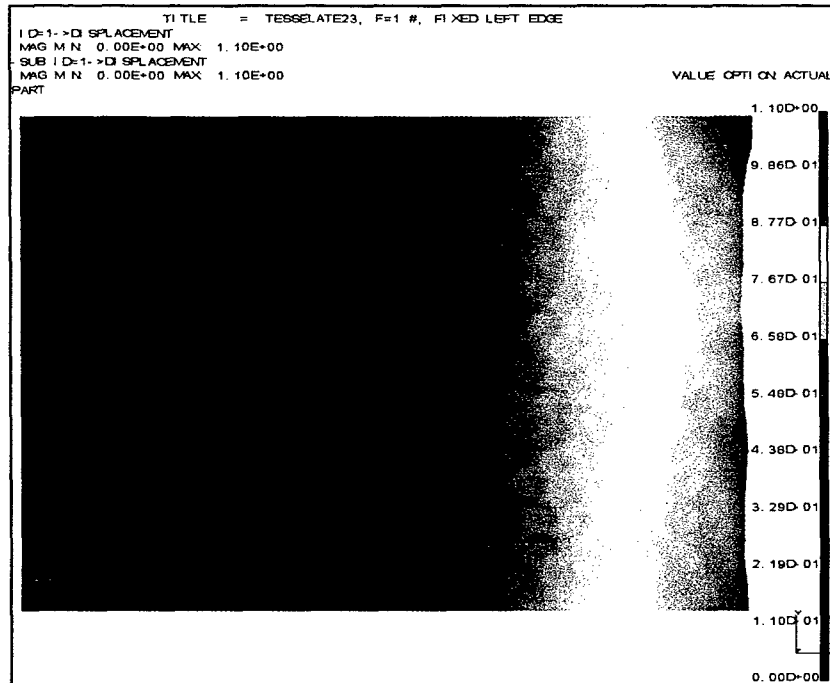


Figure 70 FEA Model, Predicted Displacement, Uniform Edge Load Applied at Right Side of Specimen

imaging techniques is planned which will provide time domain displacements of individual fibers for a sample under continuously increasing edge load. The model results can be correlated to these results to improve the viability of the model for strength and fracture based failure predictions.

At time of writing, algorithms have been successfully developed to automatically generate FEA meshes using measured fiber centers of a composite laminate specimen. The FEA models have been utilized for predictions of stress, strain, and displacement of sample specimens with specific fiber locations and uniform edge loads. Preliminary analyses of crack growth predictions have also been investigated, although additional optimization of the FEA mesh is required to improve these predictions. The developed technique provides a new tool for investigation of the contribution of subscale fiber structure to macro composite strength.

The development of the automated mesh generation tool described above is believed to represent a major contribution of this research. This capability, which has been integrated with the automated image analysis tool, will allow rapid, convenient and realistic determination of fiber architecture effects in fiber composite laminate elements comprised of large numbers of fibers. The demonstration analyses presented in Figures 67 to 69 show the capability of this tool to accurately represent strain and stress flow paths within complex fiber architectures. The artificial regularity of profiles generated using the earlier analyses based on ideal hexagonal grids is eliminated in this computational arrangement.

In Phase II of the MEANS initiative a technique known as Digital Image Correlation will be used to determine actual stress and strain profiles, and with successful completion

such an effort the capability to experimentally verify model output at appropriate length scales will exist for the first time. This technique relies on tracking algorithms that allow minor movements in magnified images of materials under stress to determine complex strain fields. It is therefore the perfect experimental analog to the numerical modeling being carried out in this project. The implications in terms of the ability to interrogate existing failure development theories are very broad ranging. For the first time a modeling capability will exist that will allow analysis to be conducted at the same length scale as the experimental sample. To be more precise it will allow the *actual sample* to be accurately modeled.

3.4 Statistical Analysis

Statistical analysis techniques were sought in this program that will allow the essential features of material variability to be represented in a fashion that clarifies its impact on structural performance. Preliminary analysis of fiber packing data provided a number of candidate statistical parameters, and later effort was devoted to identifying potential links between observed microstructural variation and statistical scatter in test data. One key benefit of Voronoi cell analysis is that it allows parameters such as fiber volume fraction, nearest neighbor distance and number of nearest neighbors to be calculated on the scale of the fiber. Standard statistical parameters can therefore be calculated for different fiber arrangements to determine the basic structure of the data. For example, some sample populations can be conveniently interrogated by computation of Cumulative Distribution Functions (CDF) or Probability Density Functions (PDF) of parameters of interest. CDF is defined as simply the probability that some variable (volume fraction, fiber spacing, etc.) assumes a value less than or equal to some value x . It is expressed as;

$$\text{CDF} = F(x)$$

The probability density function is then simply the derivative of CDF and is the probability of the variable x having a certain value. It is therefore given by;

$$f(x) = \frac{dF(x)}{dx}$$

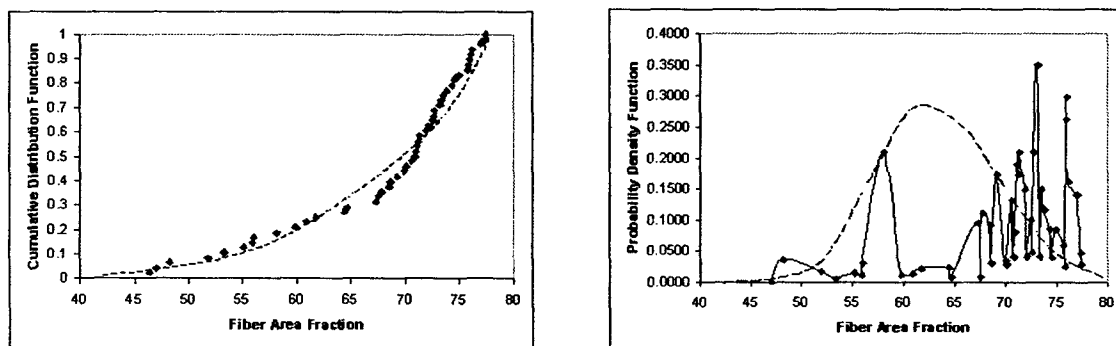


Figure 71 Cumulative Distribution Function and Probability Density Function data for Fiber Area Fraction in Sample Microstructure

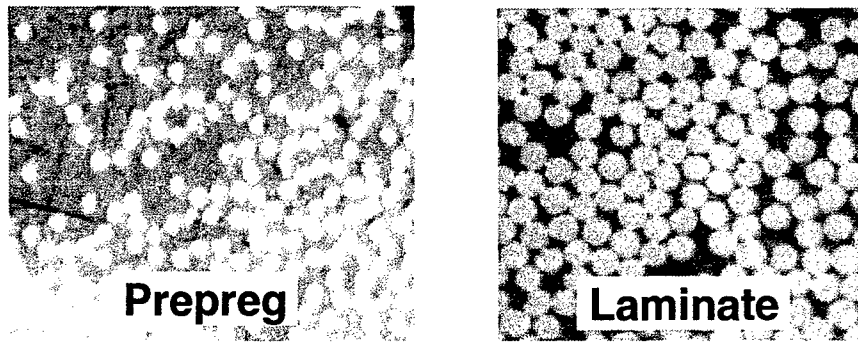


Figure 72 Micrographs of uncured graphite epoxy prepreg material and laminate fabricated by conventional autoclave processing

Figure 71 shows these functions calculated for fiber area fraction based on an AOI containing roughly 50 fibers. In both cases the general data trend expected from a Poisson Distribution (often used to describe fiber dispersion in composites) is shown. While the CDF shows little promise in describing the material variation, the PDF exhibits some of the elements required of statistical tests for fiber packing data. For instance, the peaks in the data suggest a preference for certain packing densities that may be quite disparate in value. While it is not clear which tests or parameters will be most competent to describe the variation, it is likely that some correlation with test data may be identified, if test length scales match those of the analysis. Use of such statistical methods may also play a key role in identifying appropriate length scales for structural analysis.

An illustration of how the automated image analysis tool might be used to generate data that will allow the structure of fiber packing data to be analysed is given in Figures 72 to 74. Figure 72 shows images of uncured YLA graphite/epoxy prepreg material and a laminate processed from this prepreg by standard lay-up and autoclave cure procedures (100 psi at 350°F for 4 hours). Figure 73 shows the corresponding fiber volume fraction maps for both microstructures. The fvplot program outputs fiber volume fraction data for all Voronoi cells in the map to a text file that can be imported into spreadsheets or other statistical analysis software packages. This procedure is illustrated in Figure 74

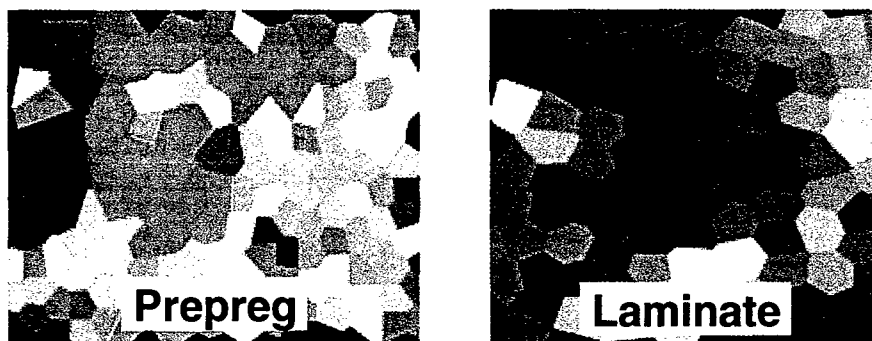


Figure 73 Fiber volume fraction maps for uncured prepreg and laminate micrographs shown in Figure 72

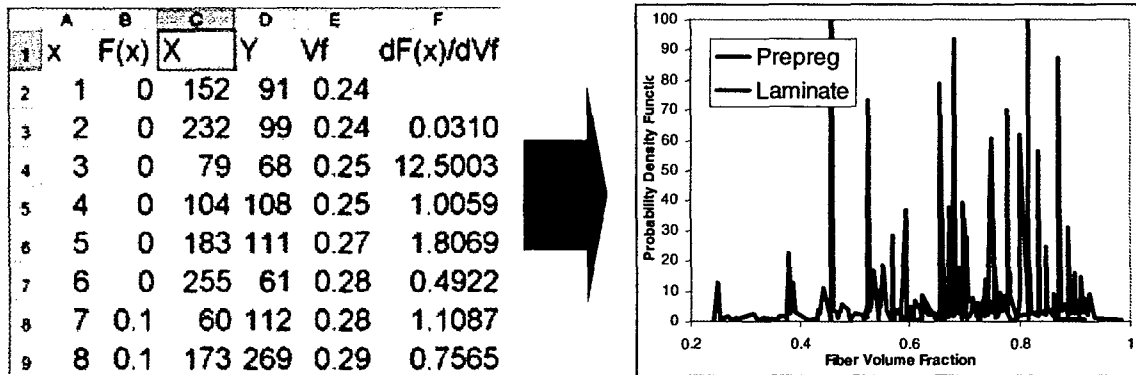


Figure 74 Example of output from automated image analysis tool being used to generate statistical data

which shows the fiber volume fraction data that is the output from the automated image analysis tool being operated on using an Excel spreadsheet. In this case the probability density function for fiber volume fraction is plotted for both the uncured prepreg and laminate images shown in Figure 72. While representing a very basic and unsophisticated analysis these data show interesting and illustrative features. Peaks in the data sets show the tendency to development of 'domains' of fiber volume fraction. Such data attributes are seen in both the prepreg and laminate numbers. This suggests that there may be a statistical mapping that would allow the final (processed) architectural parameters to be predicted from the starting point. This possibility, along with the supposition that patterns identified in packing data may influence the stochastic features of performance parameters, dictates that significant emphasis in follow on work be placed on identifying or developing statistical test techniques that allow such common patterns to be uncovered. Many pertinent techniques already exist. For instance, pattern recognition is a discipline that seeks to uncover what may be obscure trends in large amounts of data (in this case spatially varying fiber volume fraction). Data mining is a technique designed to extract certain features out of large databases and compare trends in different types of data. It is used in product marketing disciplines to predict purchasing trends based on personal characteristics. It might be of use in the current context to test whether trends in failure data could be related to micro features.

In neural networks (NN) certain types of data may be used to train a NN code to identify trends and then search for these trends in other types of data (again strength data and Vf data). Set theory is used (in this context) to describe the basic structure of the data. An important parameter in set theory is the Hausdorff dimension which essentially determines the dimensionality (1,2,3) of a given shape or data set. In the follow on program it might be used to determine whether sufficient parameters (Vf, fiber spacing etc.) are being used to describe the trends in a large (say strength) dataset. Finally, discriminant factor analysis is aimed at determining the significance of selected parameters in describing a large dataset.

Whatever statistical test technique is used to uncover relationships between raw material architecture and final laminate configuration and associated performance (if they exist), the combination of tools developed in this program allows experimentally verifiable

analysis to be carried out at a range of different length scales. Very large micrographs have been prepared for both uncured and cured laminates, containing hundreds of thousands of fibers. These cannot practically be presented in this report (because of both spatial and computer memory limitations) but they will yield data from length scales ranging to that of the fiber to, effectively, that of a laminate. Such a capability will be invaluable in determining the impact of microstructural features on performance. The planned application of Digital Image Correlation to such analysis provides, perhaps, the last piece of the puzzle, in that it will allow the development of experimental data on length scales that are appropriate to the analysis.

4.0 Summary

This program has provided an opportunity to assemble a suite of analysis tools and experimental techniques that, in combination, allow the effect of variations in microstructural characteristics of prepreg composites on resultant performance parameters to be determined. A microstructural characterization technique, based on Dirichlet planar tessellation, was shown to provide a convenient means of representing architectural variation in terms of fiber volume fraction distributions. An automated image analysis tool was developed that provided a new capability to rapidly and conveniently analyze composite microstructures, and generated output data forms that can easily be interfaced with common statistical analysis packages. This tool allows fiber center locations to be determined from micrographs in a fashion that is largely independent of image quality. This provides the data necessary to perform the Dirichlet tessellation of composite microstructural space, yielding the Voronoi cells that are used to calculate the spatially varying fiber volume fraction maps.

Fiber center data, that are principal outputs of the image analysis tool, were used to develop an automated Finite Element Grid generation code that was then used to analyze the effect of fiber arrangements on stress and strain distributions within loaded composite structures. Preliminary results showed that fiber packing arrangements can have a strong influence on microcrack development.

Micrographs generated from laminates processed from prepreg materials supplied by the program subcontractor, YLA Inc., were analyzed using the automated image analysis tool and some indication of a link between microcrack developed and local fiber volume fraction gradient was uncovered. The tool was also used to analyze micrographs published in the open literature. The quality of these older images did not present a problem for the developed code and similar trends to those suggested by analysis of 'in-house' samples were identified.

A two stage prepreg polishing technique, that allows the initial fiber architecture to be determined, was also developed. This provides the capability to determine any links between prepreg architecture and final laminate microstructural configurations to be determined.

5.0 References

- 1 Gregory, P Dillon & Bryan D. Mayrides, "Influence of Composite Microstructure on Structural Performance," SAMPE 35th Annual Technical Conference in Dayton, Ohio, September 28th to October 2nd, 2003.
- 2 Gutowski, T. G., and Dillon, G., "Elastic Deformation of Lubricated Aligned Carbon Fibers: Comparison of Theory and Experiments," *Journal of Composite Materials* Vol.26, No.16 1992, p2330.
- 3 Abry, J.C., Choi, Y.K., Chateauminois, A., Dalloz, B., Girard, G. and Salvia, M., "In-situ Monitoring of Damage in CFRP Laminates by Means of AC and DC Measurements", *Composites Science and Technology*, Vol. 61, 2001 pp855-864.
- 4 Laferie – Frenot. M.C., Henaff – Gardin, C. and Gamby, D., "Matrix Cracking Induced by Cyclic Ply Stresses in Composite Laminates", *Composites Science and Technology*, Vol. 61, 2001 pp2327-2336.